Dynamic Calibration of Force Balances

David J. Mee
Centre for Hypersonics
Department of Mechanical Engineering
The University of Queensland. Australia.

Abstract

This report describes different techniques for the calibration of stress-wave force balances. A short introduction is presented on how deconvolution can be used to infer aerodynamic forces on models in impulse hypersonic wind tunnels along with the theory behind the different calibration techniques. Simulations of calibration tests and recovery of forces using the different calibration techniques are performed to show the accuracy with which impulse responses can be found and aerodynamic forces resolved. Bench tests for a single-component stress-wave force balance and experiments in the T4 shock tunnel using the same balance are used to demonstrate the suitability of different calibrations. It is shown that the impulse response derived from tests involving the cutting of a fine wire which suspends the model and force balance agrees very well with impulse responses derived from calibrations made using an impact hammer. However, some of the methods used for impact calibrations are very sensitive to noise on the measurement signals. Techniques for minimizing these effects and for dealing with the noise to reduce errors are also presented.

Contents

Nomenclature

a	Amplitude of step
A	Reference Area
C_D	Drag coefficient
d	Height above datum line
D	Drag force
$\mathbf{F}$	Force during impact
g	System impulse response
G	Laplace transform of impulse response
h	Enthalpy
$\mathbf{i}$	Unit vector in x direction
$\mathbf{I}$	Impulse
l	Length of pendulum
m	Mass of impactor
M	Mach number
p	Pressure
R	Gas constant
Re	Reynolds number
T	Temperature
s	Laplace transformed time
S	Area under force vs time curve
t	Time
T	Duration of pulse
u	System input
U	Laplace transform of input
v	Speed
$\mathbf{v}$	Velocity
x	Horizontal coordinate
y	System output
Y	Laplace transform of output
γ	Ratio of specific heats
δ	Delta function
Δx	Distance from model in x direction
ρ	Density
τ	Shifted time

Subscripts

∞	Free-stream condition
B	Ball impactor
CT	Compression tube
i	Initial position
f	Final position
M	Model
Pit	Pitot
res	Reservoir
s	Nozzle supply region

ST Shock tube

Superscripts

$*$ Immediately after impact

Chapter 1

Introduction

The measurement of aerodynamic forces on models in hypersonic impulse facilities has been restricted in the past because of the time it takes for the test model to reach a state of force equilibrium with its support mechanisms (Bernstein, 1975). Conventional force balances rely on damping mechanisms and/or filters to reduce the effects of vibrations, associated with the sudden application of aerodynamic forces when the flow starts or when the model is injected into the flow. In impulse facilities, particularly high-enthalpy facilities, the duration of the test flow may be insufficient for such vibrations to be damped before the end of the test and the period of vibrations can even exceed the test time.

Various techniques can be used to address these problems. The model can be made small and light and the force balance very stiff so that the natural frequency of the system is high (e.g. Jessen & Gronig, 1989). Accelerometers can be placed on the model and can be used to detect vibrations that can then be used to compensate the strain signals from the force balance (e.g. Carbonaro, 1993). Another possibility is to to measure the acceleration of the model and use flexible supports for the model (e.g. Joshi & Reddy, 1986) or to let the model fly freely during the test (e.g. Naumann *et al.*, 1993). This eliminates the effect of a support mechanism decreasing the natural frequencies of the system. The natural frequencies are then set by the model size, its stiffness and the speed of stress waves in the structure of the model. A small model keeps these frequencies high and a light model leads to larger acceleration signals.

When force measurements are required on models of larger size and mass in impulse facilities, the period of the lowest natural frequency of the force balance can become of similar order to the duration of the test flow. For such conditions, it is possible to use system identification and inverse techniques to include the system dynamics in the analysis of the force balance signals to determine the time history of the aerodynamic forces on the balance. One such technique, the stress-wave force balance (SWFB) technique, was proposed by Sanderson & Simmons (1991). Development of the stress-wave force-balance has continued at The University of Queensland over the last decade (see Tuttle *et al.*, 1995; Mee *et al.*, 1996; Smith & Mee, 1996*a*; Smith *et al.*, 2001).

When an aerodynamic load is suddenly applied to a model in the test section of an impulse facility, stress waves are initiated within the model. These stress waves propagate and reflect within the model and its support structure. During the short period of steady flow, no steady state of force equilibrium can be achieved between the model and its support. The principle of the SWFB lies in accepting the fact that no steady state is achieved. Then the time histories of the aerodynamic forces on the model which caused the stress wave activity are determined from the measurement (at one or more locations on the model or its support structure) of the strain time histories.

The system of the aerodynamic model and its support structure behaves as a linear dynamic system (for forces which lead to linear strains). Such a linear system is shown schematically in Fig. 1.1. If the load applied to the model is $u(t)$ and some strains are developed within the model and its support structure and these strains are measured giving a signal, $y(t)$, then the relationship between the input and the output can be written as

$$y(t) = \int_0^t g(t - \tau)u(\tau)d\tau. \tag{1.1}$$

Here the function relating the input and output is the impulse response function, $g(t)$.
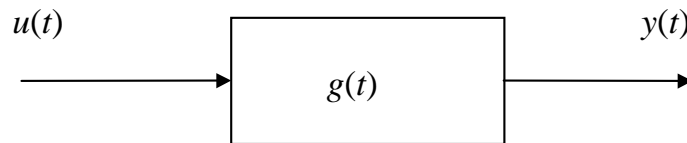

Figure 1.1: Schematic of a linear system representing a force-wave force-balance

If the system characteristics (in the form of the impulse response function) are known, then a deconvolution procedure can be used to determine the time history of the applied load from the time history of measured strain.

The purpose of this report is to investigate methods for experimental determination of the impulse response function. The background theory behind the different calibration techniques used in the report is presented in chapter 2. Simulations of the calibration of a single-component stress wave force balance, using the different calibration techniques, are presented in chapter 3. This chapter also includes simulations of some of the problems that may be encountered using pulse calibration techniques. Results from experiments to calibrate a single-component force balance using the different techniques presented in this report are presented in chapter 4. Cross checks on the different techniques are also presented. The calibrated force balance was tested in the T4 shock tunnel. Results from those tests are used to compare the different calibration techniques and the outcomes are also presented in chapter 4.

There are three appendices. Appendix A shows some of the problems that may arise in dynamic calibration of force balances. Appendix B presents the theory for a pulse calibration technique that uses the impact of a pendulous mass to apply a pulse to a model on a force balance. This technique has not been applied to the force balance tested in chapter 4. Appendix C presents the background to using a measured Pitot pressure signal along with a measured force signal to determine the variation of force coefficient with time during an experiment in a hypersonic flow.

Chapter 2

Theoretical background

2.1 Determination of the impulse response from a step response

One method for experimentally determining the impulse response is to measure the output signal generated by a step change in the input to the system. This is called the step response of the system and the impulse response can be determined by differentiating the step response with respect to time and scaling the result appropriately. This can be shown by taking the Laplace transform of eq. (1.1) to obtain

$$Y(s) = G(s)U(s),\tag{2.1}$$

where $Y(s)$, $G(s)$ and $U(s)$ are the Laplace transforms of $y(t)$, $g(t)$ and $u(t)$ respectively. Let the input be a step of magnitude a starting at time $t = 0$,

$$u(t) = \begin{cases} 0 & t < 0, \\ a & t \geq 0. \end{cases}\tag{2.2}$$

The Laplace transform of this input is a/s and eq. (2.1) becomes

$$Y(s) = \frac{aG(s)}{s}\tag{2.3}$$

Inverting this gives

$$y(t) = a \int_0^t g(\tau)d\tau,\tag{2.4}$$

or

$$g(t) = \frac{1}{a}\frac{dy(t)}{dt}.\tag{2.5}$$

Therefore the impulse response can be determined from the response of the system to a step of magnitude a.

The ideal step response excites all frequencies of the system. However the amplitudes of excitation are heavily weighted to low frequencies (see, e.g., Reed, 1998). This can be seen by noting that the amplitudes of the sinusoidal Fourier components that go to make up a step have amplitudes that vary inversely with frequency. As noted by (Reed, 1998), "While complete representation of the ideal step also requires all frequencies, the amplitudes at the higher frequencies rapidly become infinitesimal, therefore negligible."

If a finite element model of the SWFB arrangement is made, step responses can be determined by dynamic analysis. This has been used extensively at UQ in design of SWFB (e.g. Daniel & Mee, 1995; Smith *et al.*, 2001). In some cases impulse responses derived by differentiating step responses obtained using finite element analysis have been used to deconvolve wind tunnel data (Sanderson & Simmons, 1991; Smith & Mee, 1996*a*). In order to avoid any effects due to modelling approximations used in the finite element analysis, it is preferable to measure the step response experimentally.

To demonstrate how to obtain a step response experimentally, consider a single-component SWFB, such as that of Sanderson & Simmons (1991), consisting of an axisymmetric model attached to a long stress bar aligned with the axis of the model (Fig. 2.1). An approximate step change in axial load on the model can be applied by attaching a fine wire to the tip of the model, applying a load to it, and then cutting the wire. This requires the right hand end of the stress bar (in Fig. 2.1) to be held so that free-body motion of the arrangement does not occur when the load is applied via the wire. Two possible calibration arrangements are shown in Fig. 2.2 and 2.3(a) where a known mass is attached to the wire to apply a known load to the model. In Fig. 2.2 the model is supported horizontally (as it is in the test section of the wind tunnel) and the wire passes over a pulley to the mass. The wire is cut close to the model. In Fig. 2.3(a) the axis of the balance is vertical and the balance is supported by a wire attached to the end of the stress bar. Each of these techniques has been used to obtain step responses.
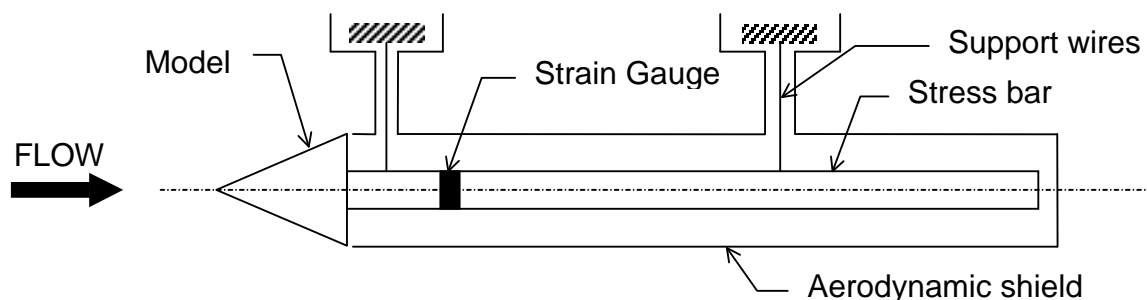
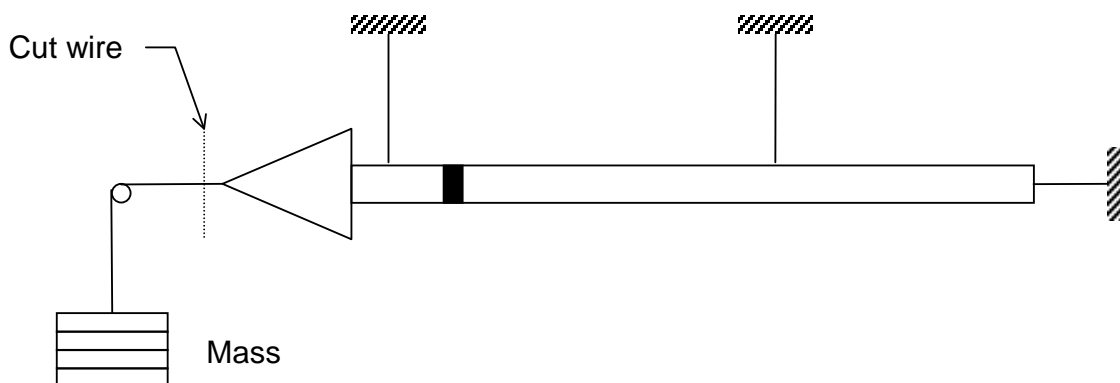

Figure 2.1: Single-component stress-wave force-balance

Figure 2.2: Horizontal Calibration

7

A deficiency of the calibration arrangements in Figs. 2.2 and 2.3(a) is that the end of the stress bar must be supported. In the experiment this end is free (as in Fig. 2.1). The impulse response derived from a step response for one of these arrangements will then only be valid for the period of time it takes for a stress wave to travel from the tip of the model, reflect from the end of the stress bar and return to the strain measurement location. (For a 300 mm aluminium model, a 2 m brass stress bar and the strain gauge located on the brass bar 200 mm from the model, this time would be 1.15 ms.) Thus the maximum length of tunnel signal that could be processed with such an impulse response would be limited to this time.

This deficiency can be overcome by the calibration arrangement shown in Fig. 2.3(b). Here the SWFB is again supported vertically but the load applied to the tip of the model is the weight of the SWFB and the end of the stress bar is free. When the wire is cut, the load is suddenly removed at the tip and the arrangement falls. During the period of free-fall there is no load on the model and a step response valid for the tunnel experiments is obtained for a longer period of time. The magnitude of the applied step is set by mass of the model and stress bar.

2.2 Determination of the impulse response from a pulse test

Another method for determining the impulse response is to try to apply a true impulse to the system and to measure the response of the system to it. This is an attractive method for exciting the system because a true impulse (delta function or Dirac function) is equivalent to applying the set of all harmonic functions simultaneously for all frequencies (see, e.g. Dieulesaint & Royer, 1980, pp. 28-29). Thus, it can potentially provide as much information as a point-by-point analysis for every frequency. Of course, there are practical limitations to this, as discussed below.

Consider an input to the system which has the form of a perfect impulse. i.e. $u(t) = S\delta(t)$ where $\delta(t)$ is the unit impulse function,

$$\delta(t) = \begin{cases} 0 & t \neq 0, \\ \infty & t = 0, \end{cases} \tag{2.6}$$

with $\int_{-\varepsilon}^{+\varepsilon} \delta(t)dt = 1$ as $\varepsilon \Rightarrow 0$. S is the area (under a force-time curve) of the pulse. Then from eq. (1.1)

$$y(t) = \int_0^t g(t-\tau)S\delta(\tau)d\tau. \tag{2.7}$$

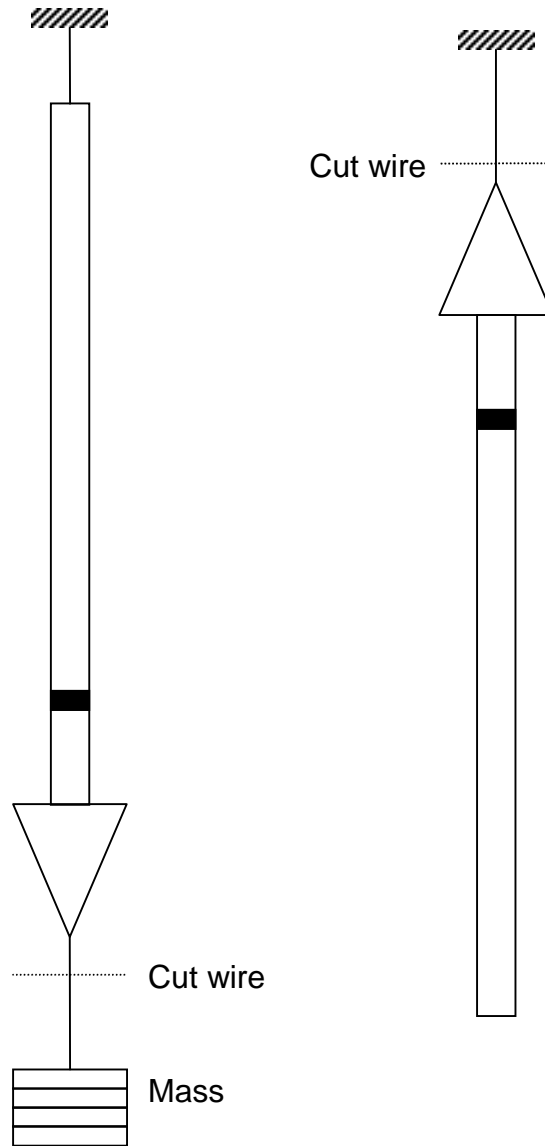Since the convolution integral is commutable, this can be rewritten as

$$y(t) = \int_0^t g(\tau)S\delta(t-\tau)d\tau = S\int_0^t g(\tau)\delta(t-\tau)d\tau. \tag{2.8}$$

Noting the shifting property of the delta function,

$$\int_a^b f(\tau)\delta(t-\tau)d\tau = f(t), \tag{2.9}$$

the final result is

$$y(t) = Sg(t). \tag{2.10}$$

(a) Vertical calibration.   (b) Free-end calibration.

Figure 2.3: Vertical calibration techniques.

Thus the output to a perfect pulse of area S is the true impulse response scaled in magnitude by S.

A perfect impulse cannot be achieved in practice and the question which arises is how short or sharp does an impulse need to be in order to produce essentially the same response as the perfect impulse. The relevant timescale is the characteristic time of the system under test. As demonstrated in Doebelin (1980), when the period of the pulse is short in comparison with the characteristic time of the system, the details of the shape of the pulse make no difference to the response obtained and only the area of the pulse is important. When the period of the pulse is not short, the response is dependent on the shape of the pulse.

One mechanism for calibrating a SWFB is to apply a short force pulse at a point on the model using an instrumented impactor. Such an arrangement is shown schematically in Fig. 2.4. The impactor, shown as a hammer, is instrumented to indicate the time-history of force applied during the pulse. If the period of the pulse is short in comparison with the characteristic time for the balance and the magnitude of the pulse is measured, the impulse response can be determined from the system response using eq. (2.10). Implementation of such a system is described in section 3.2.
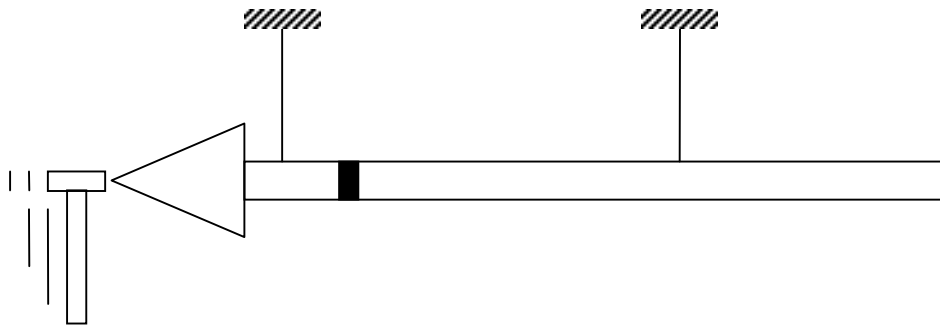

Figure 2.4: Pulse Calibration

Another way to apply a short pulse is to suspend a small mass as a pendulum and allow it to strike the test model. Unlike the hammer calibration technique discussed above, the time history of force during the impact is not measured. However, by noting the initial potential energy of the pendulous mass and how far it rebounds after impact, it is possible to determine the magnitude of the impulse that is applied to the model by the impact. This technique has not been applied in the present investigation but the background theory is presented in Appendix B.

2.3 Determination of the impulse response by measuring the response to an arbitrary input

Equation (1.1) indicates that the relationship between an input $u(t)$ and the associated output $y(t)$ is in the form of a convolution integral. This suggests that by applying any measurable transient input to the system and noting the response, deconvolution techniques could be used to determine the impulse response, $g(t)$. There is a limitation to this method that can be explained in terms of the frequency spectra of the input to the system and the impulse response. There is a loss of accuracy in applying deconvolution techniques at

frequencies where the impulse response is non-zero but the applied input is small. At such frequencies any measurement or digitization errors in the input or output can lead to an unreliable impulse response being calculated. Thus the frequency content of the input and impulse response must be considered when trying to determine $g(t)$ from an arbitrary input. An input signal that has a shape similar to that expected in an experiment should be suitable for calibration. However, it is not necessary to have the same time history for the calibration input and the experiment input in order for deconvolution to be successful.

One type of input that could be used to determine the impulse response by deconvolving the output signal with the input signal is the pulse input discussed in section 2.2. Instead of dividing the response to the pulse input by the impulse applied as discussed in section 2.2, if the shape of the pulse is measured as well as its magnitude, the measured input pulse signal could be used to deconvolve the measured output signal to infer the impulse response. While this input does not resemble that expected the force time history on a model in a test in a hypersonic impulse facility, it is shown in chapters 3 and 4 that this can lead to a good estimate of the system impulse response. Such a calibration technique can potentially provide details of the impulse response for higher frequencies than can the method of simply dividing the balance response by the magnitude of the applied impulse. This is because the shape of the pulse can be taken into account.

Chapter 3

Simulations

In order to demonstrate the techniques discussed in chapter 2 for determination of the impulse response for a SWFB a series of simulations has been carried out. An impulse response representing that which would be obtained for a short, conical model on a single-component (drag) SWFB (such as the balance in Fig. 2.1) is shown in Fig. 3.1. In fact this is the response from an pulse of duration about 200 μs applied to the model described in chapter 4. For the purposes of the present simulations, this is taken to be the true impulse response of the SWFB being considered. Because it is from a pulse test, this impulse response does not contain all the high-frequency information that would be obtained for a model such as that in chapter 4 but is useful here because it is easier to visually compare different impulse response because they are not dominated by high-frequency content. The effects of neglecting very high-frequency content in the impulse response is considered in section 3.2.2.

The time scale chosen for the pulses and response signals spans a total period of about 8 ms. In all the simulations presented in this chapter, the signals have been discretized at a time step of 5 μs. The scales shown for the loads, system responses and impulse responses are arbitrary. Working in a system where the time is measured in s, the input signal is a force in N and the output response signal is measured in V, the units of the impulse response will be V/N/s.

Also considered in the simulations is an idealized wind-tunnel drag signal (Fig. 3.2). This is an idealized form of the signal obtained in the T4 shock tunnel at The University of Queensland. It shows an initial overshoot (associated with nozzle starting processes), a period of steady drag and then a period of continually reducing drag (associated with the end of the test period). A simulated output signal that would be obtained from the SWFB for such an input signal can be obtained by convolving the impulse response in Fig. 3.1 with the input signal in Fig. 3.2 using eq. (1.1). The result is shown in Fig. 3.3.

As a benchmark for subsequent comparisons, the output signal in Fig. 3.3 has been deconvolved with the true impulse response to show how well the original input signal is recovered. The deconvolution technique used is the functional minimization with extended conjugate gradient method of Prost & Goutte (1984). This is an iterative procedure and the deconvolved signal, obtained after 200 iterations, is shown in Fig. 3.4. This recovered signal is compared with the original input signal of Fig. 4b and it can be seen that the details of the applied load are recovered well. There is some high frequency noise on the signal which reduces as the number of iterations is increased. The fact that the recovered signal drops to zero for the last 300 μs can be explained in terms of the shape of the impulse response. The load is applied at the tip of the model. Since the strain gauge is remote from the point of application of the simulated load and stress waves travel at a finite speed there is a time delay between application of the load and when the associated stress waves are first detected
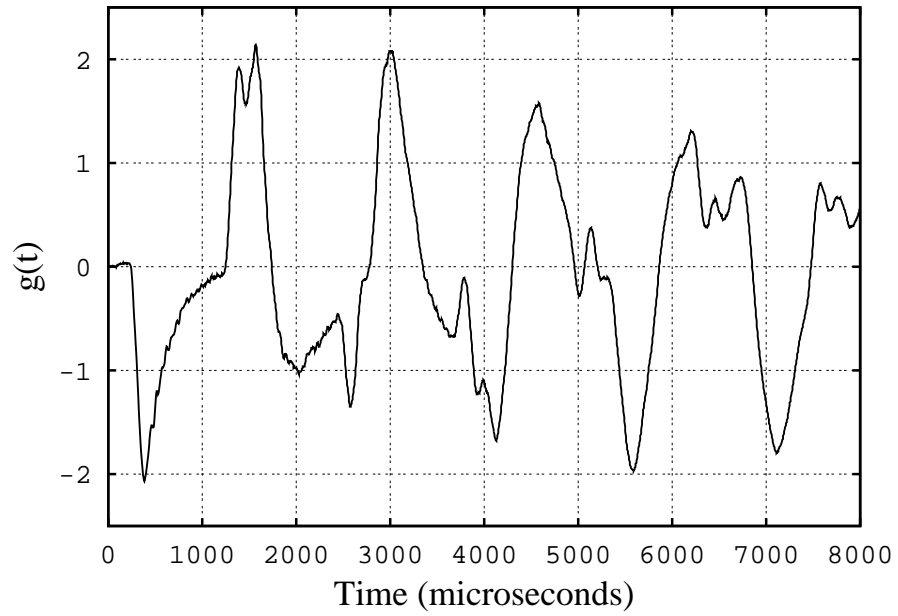
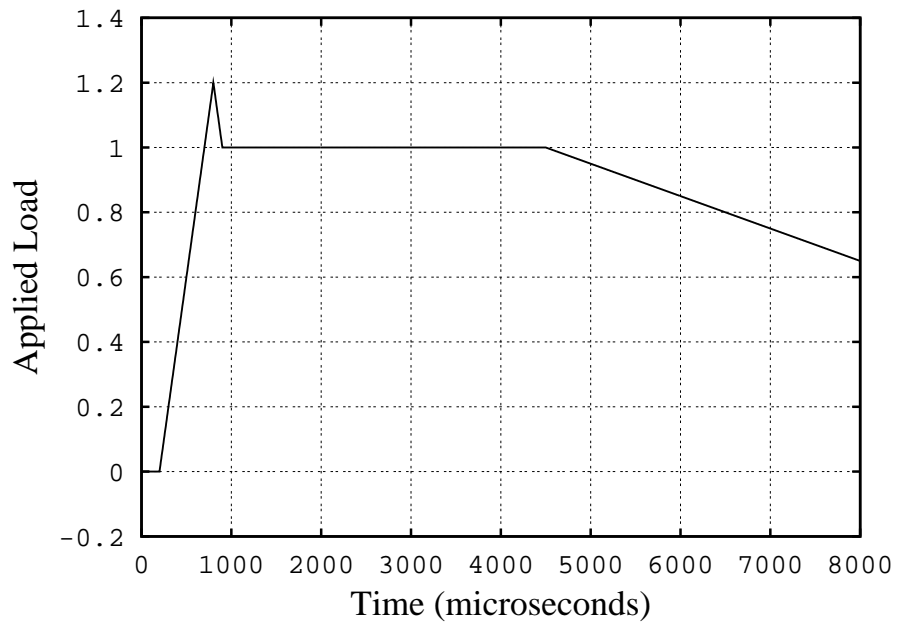Figure 3.1: "True" impulse response for simulations.

Figure 3.2: Simulated tunnel applied load signal.
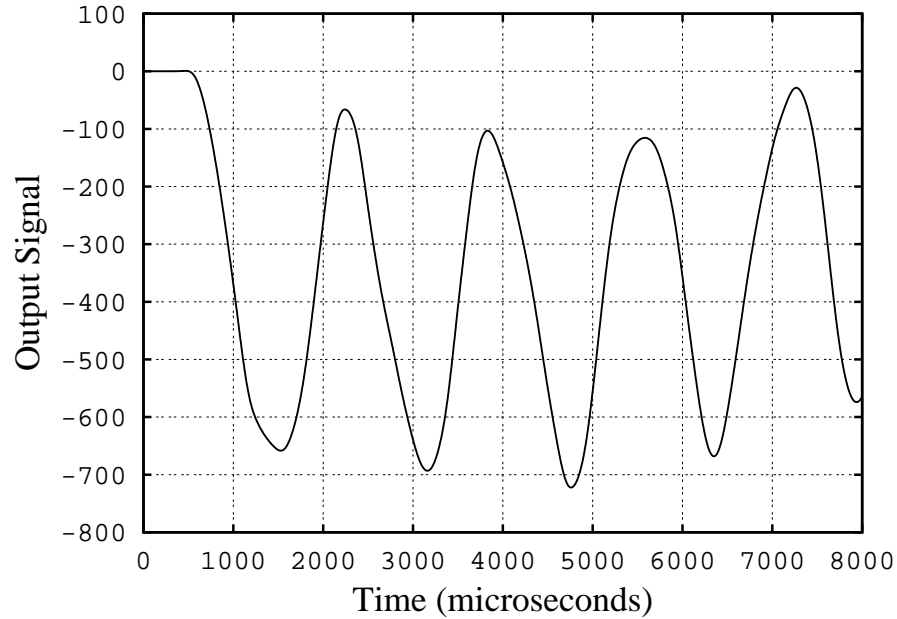
13

Figure 3.3: Simulated output signal for input of Fig. 3.2 and impulse response of Fig. 3.1.

at the gauge location. This is why the impulse response remains at zero for the first 300 μs in Fig. 3.1. When using deconvolution to reconstruct the signal which caused the simulated output signal, the last 300 μs of the input signal cannot be determined from the output signal - it is not possible to determine what the input would be for that period because the output signal would not yet have responded to that input.

3.1 Determination of the impulse response from a step response

For a system that has as its impulse response the signal in Fig. 3.1, the response to a unit step input applied at time zero can be found by performing the convolution integral in eq. (1.1) with an input signal stepping from zero to one at time zero. If this is done, the response in Fig. 3.5 is obtained. Differentiating this signal with respect to time should then recover the impulse response. This is demonstrated in Fig. 3.6. A comparison of the original impulse response with the impulse response generated by numerical differentiation of the step response shows very good agreement, the curves being indistinguishable. Thus, as expected, if a perfect step can be applied to a system, the impulse response can be found quite easily. Deconvolution of the simulated tunnel signal in Fig. 3.3 with the impulse response determined from the step response produces a recovered signal indistinguishable from that shown in Fig. 3.4, obtained with the true impulse response.

The practical limitation on the frequency content and quality of the impulse response determined from a step response lies in how short is the period over which the load can be applied to (or removed from) the model. The standard technique that has been used over the last decade at UQ to obtain a step response is the cutting of a fine steel wire either supporting the model, as shown in Fig. 2.3(b), or supporting a mass attached to the model, as shown in Fig. 2.3(a) (e.g. Sanderson & Simmons, 1991; Tuttle *et al.*, 1995; Mee *et al.*, 1996). This technique has proven adequate for most stress wave force balances used at UQ and the quality of the step is considered in section 4.2 where the result from cases where
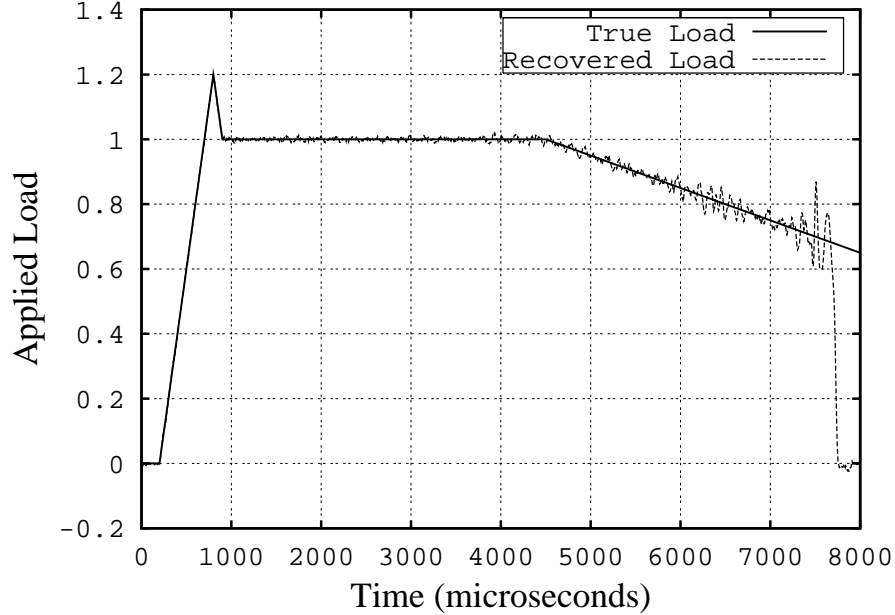
Figure 3.4: Input signal recovered by deconvolution of the output signal in Fig. 3.3 with the impulse response in Fig. 3.1. The recovered signal and the true applied load are shown.

wires have been cut have been deconvolved using impulse responses determined from pulse tests and the results show that the load is removed over a period of less than 10 μs. For very small models, such as those used in the X1 expansion tunnel where test times were as short as 50 μs (Smith & Mee, 1996a), cutting wires could not be used to obtain reliable and repeatable impulse responses. In Smith & Mee (1996a) the impulse responses used to deconvolve signals from the experiments were determined from finite element modelling.

3.2 Determination of the impulse response from a pulse test

3.2.1 Impulse response without much high-frequency content

Consider again the system with the impulse response shown in Fig. 3.1. In order to demonstrate the determination of the impulse response by measuring the response of the system to a pulse input, consider a simulated pulse that has the form of one quarter of a sinusoid,

$$u(t) = \begin{cases} \frac{\pi}{2T}\sin(\frac{\pi t}{T}) & 0{\leq}t < T, \\ 0 & t{\geq}T. \end{cases} \tag{3.1}$$

Here the pulse is of duration T and the magnitude is chosen such that the area under a curve of u vs t is unity. Such a pulse of 150-μs duration is plotted in Fig. 3.7.

Taking the normalized pulse response as the impulse response

The response of our simulated system to the input in Fig. 3.7 can be determined by convolving the pulse of Fig. 3.7 (the system input) with the "true" impulse response of Fig. 3.1 (the system impulse response). The result is presented in Fig. 3.8. This signal is compared also with the true impulse response in this figure. It can be seen that that the response to the
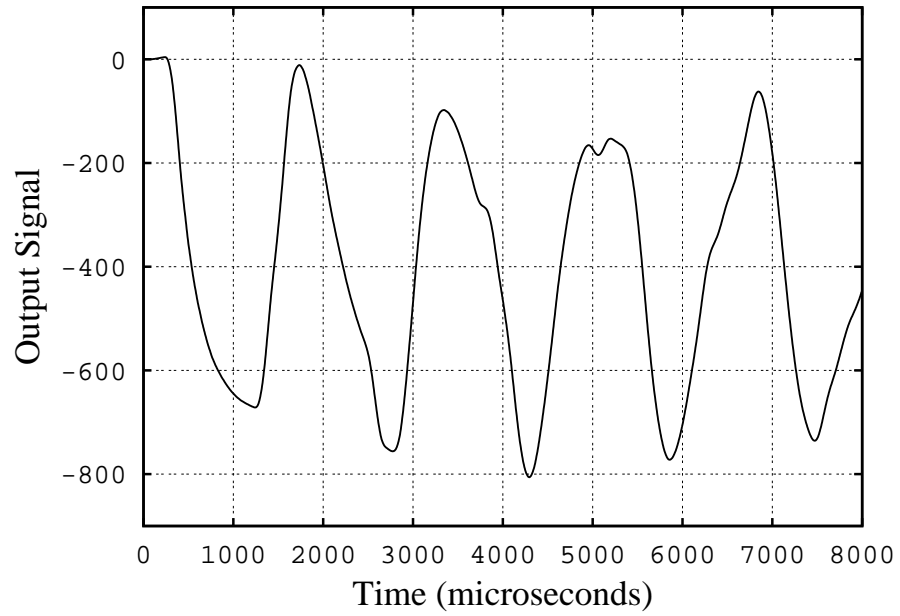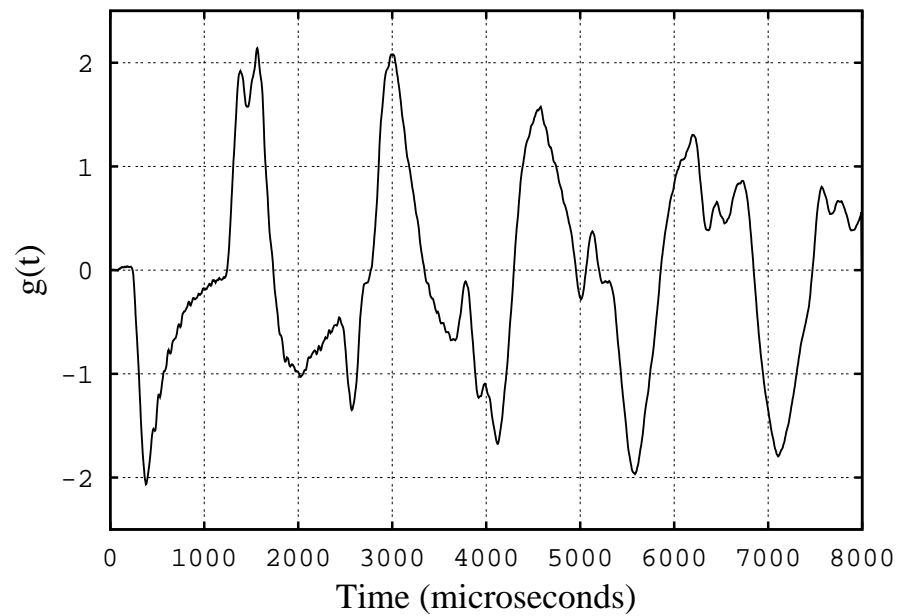
15

Figure 3.5: Simulated response to a unit step input.

Figure 3.6: Impulse response determined by differentiating the step response of Fig. 3.5.
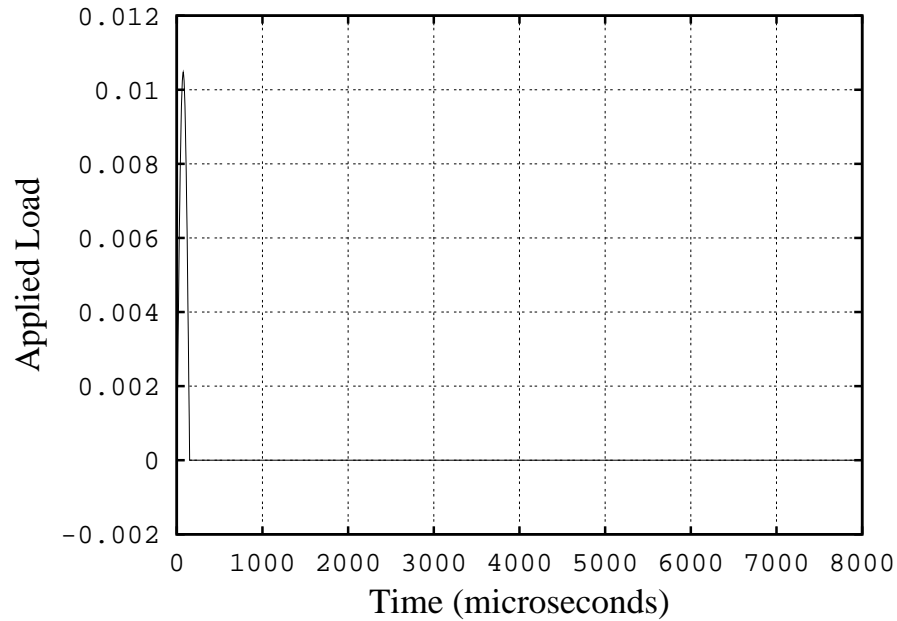
16

Figure 3.7: 150 μs duration pulse input.

short pulse is somewhat smoother than the true system impulse response and that the pulse response is shifted in time. The time-shift comes about because the pulse is not centred at time zero but at time +75 μs (half the duration of the symmetric pulse). If the pulse response is shifted by -75 μs the result in Fig. 3.9 is obtained. This result suggests that, apart from some loss of high frequency information, the impulse response obtained using this method is similar to the true impulse response.
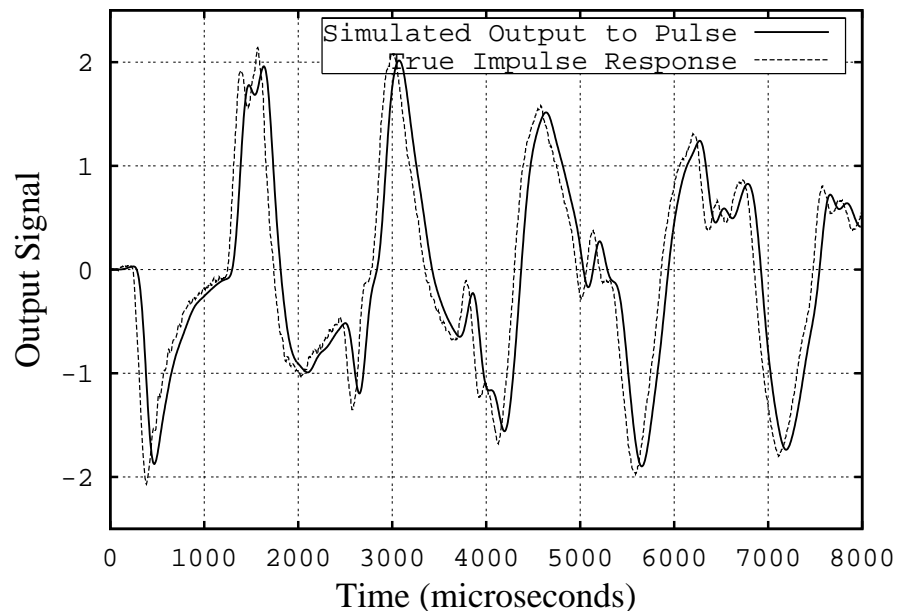

Figure 3.8: System response to pulse input compared to the "true" impulse response.

The pulse of Fig. 3.7 has a duration about an order of magnitude less than the period it takes a stress wave to travel back and forth along the length of the SWFB. The effect of a pulse of shorter or longer duration is illustrated in Fig. 3.10. In this figure a pulse of 50 μs
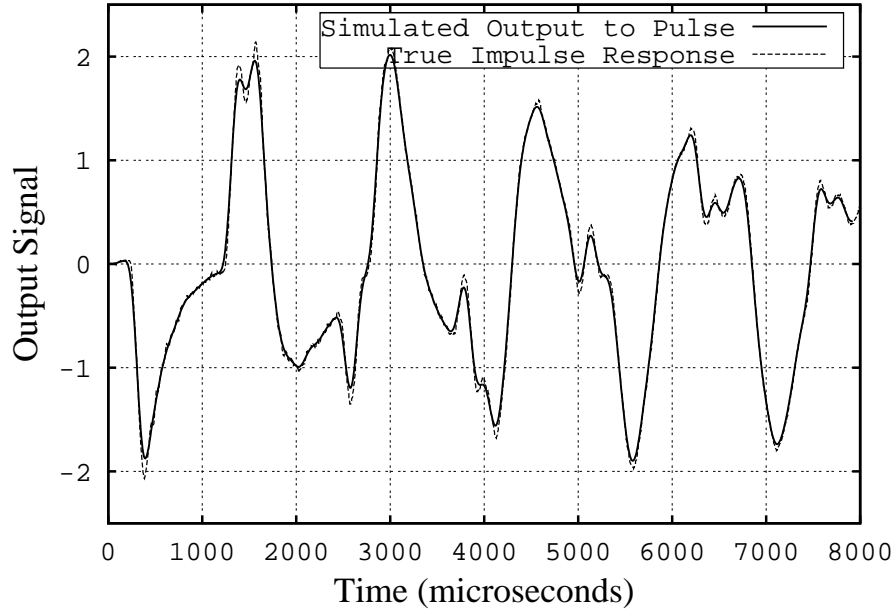
17

Figure 3.9: Pulse response shifted by 75 μs compared with the "true" impulse response.

and one of 500 μs are compared with the true impulse response. As in Fig. 3.9, the responses have been shifted to centre the pulse at time zero. The response to the short duration pulse is almost indistinguishable from the true impulse response. The response to the long pulse does not contain the high frequency information.

The three impulse responses obtained for the three pulse inputs have been used to deconvolve the simulated tunnel signal of Fig. 3.3. (Note that the impulse responses are determined from the pulse responses by normalizing the response with the area under the pulse as shown in eq. (2.10). In each of the cases simulated here, the area under the pulse was already unity, so the response to the pulse input is already the estimate of the impulse response.) The recovered input signals are shown in Figure 3.11. These results indicate that the two shorter pulses, which have periods similar to or less than the time it takes stress waves to traverse the model, can be used directly to obtain an adequate estimate of the impulse response of the balance. However, the longer duration pulse could not be used unless appropriate filtering could be applied and the associated loss in frequency response could be tolerated.

Determining the impulse response using deconvolution

An alternative method for determining the impulse response from the response of the system to a pulse is to use a deconvolution procedure in which the input to the system is known (the shape and size of the pulse) and the output of the system is measured. This has been done with the present simulated system and the simulated responses to the pulses of different width. The impulse responses determined in this way are almost indistinguishable from the true impulse response. For example, the impulse response determined for the pulse of 500-μs duration is shown in Fig. 3.12. This indicates that a pulse test can be used to determine the impulse response even if the period of the pulse is much longer than the period it takes for stress waves to traverse the model.

These results indicate that when the pulse width is short, such that all frequencies of interest in the system are excited, then a normalized pulse response will give a suitable estimate of the impulse response of the system. However, when the pulse duration is long
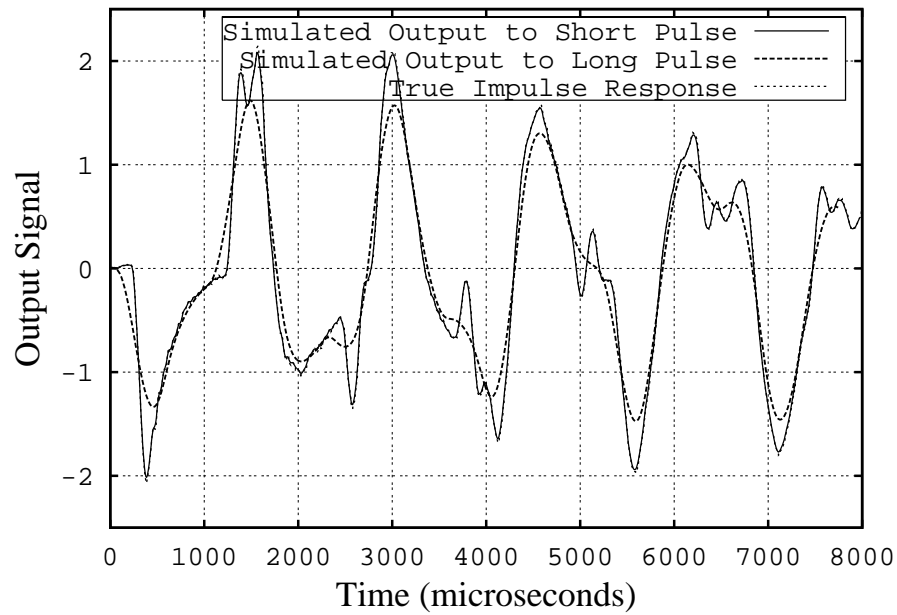
18

Figure 3.10: Responses of the system to short pulse (50 μs) and long pulse (500 μs) compared with the true impulse response.
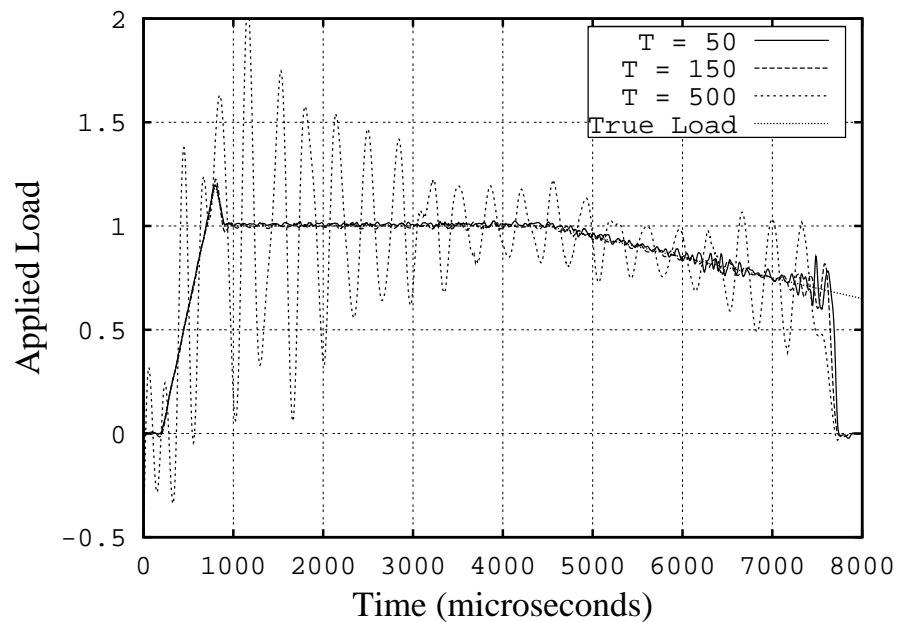

Figure 3.11: Recovered inputs for impulse responses formed from pulse responses of different pulse widths. The pulse durations shown in the legend are in microseconds.
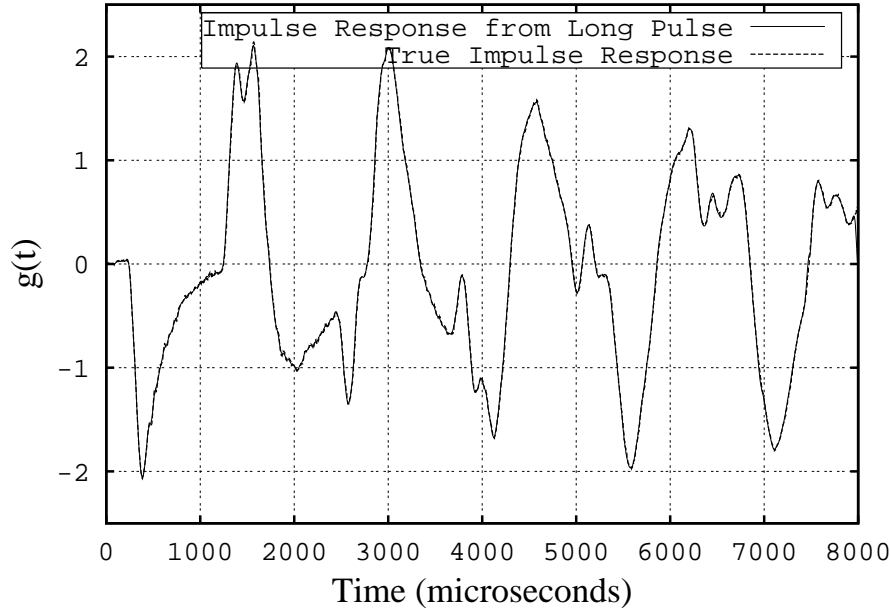
19

Figure 3.12: Impulse response determined by deconvolving signal from long pulse ($T = 500~\mu$s) compared with the true impulse response.

compared with characteristic time scales of the system, it is preferable to determine the impulse responses from pulse tests using deconvolution rather than relying on the width of the pulse being small (compare the impulse responses determined from the pulse of period 500 μs using the two techniques in Figs. 3.10 and 3.12). One limitation on this in a practical system is the influence of noise on the signals. Since deconvolution amplifies system-inconsistent noise, then there may be circumstances where it is preferable to tolerate some loss of frequency response of a force balance in order to obtain an impulse response with less noise by taking the normalized pulse response as the impulse response.

3.2.2 Impulse response with high-frequency content

As noted at the start of this chapter, the impulse response used in the simulations so far does not contain as much high-frequency information as would occur for practical implementation of a SWFB of the form shown in Fig. 2.1. It might be argued that the conclusions drawn about the suitability of calibrations using pulses of different duration could be invalid because the shorter pulses will not excite as much high-frequency in the response for the simulated system as they would in a real system. This issue is addressed here by considering an impulse response and load time history more representative of an actual SWFB.

The impulse response for the new system to be studied here is shown in Fig. 3.13. This impulse response is actually that obtained by differentiating the signal from a step response calibration for the model used in chapter 4. The calibration test was one in which the model was suspended by a fine wire, as shown in Fig. 2.3(b), and the wire was then cut. A simulated input signal, more representative of that in an actual experiment than that shown in Fig. 3.2, was formed from a Pitot signal measured during a test in the T4 shock tunnel (refer to section 4.3). This is shown in Fig. 3.14. The output signal that would be measured for this system with this load applied is obtained by convolving the impulse response in Fig. 3.13 with the applied load of Fig. 3.14. The result is shown in Fig. 3.15.

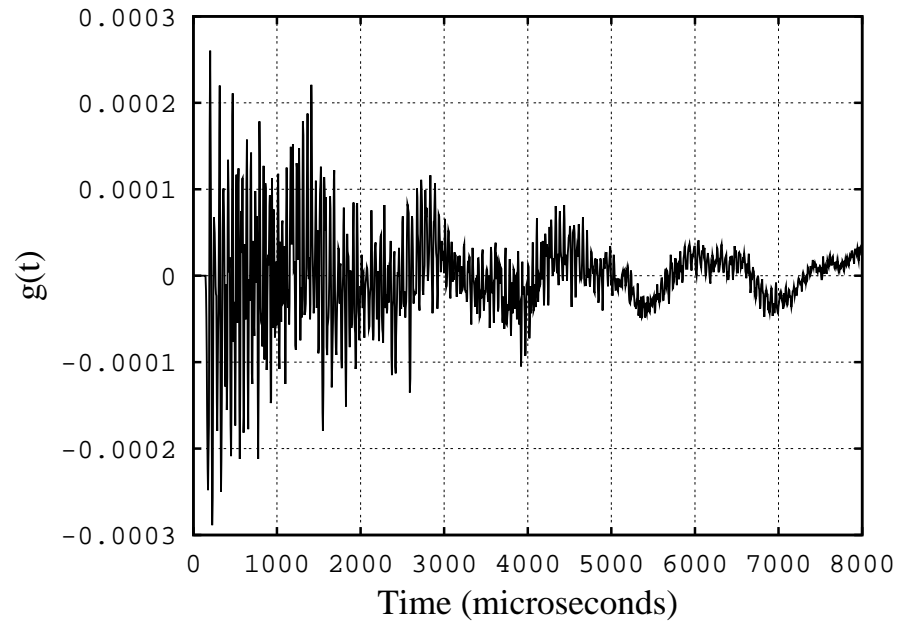A similar procedure to that applied in section 3.2 is applied to the current system to

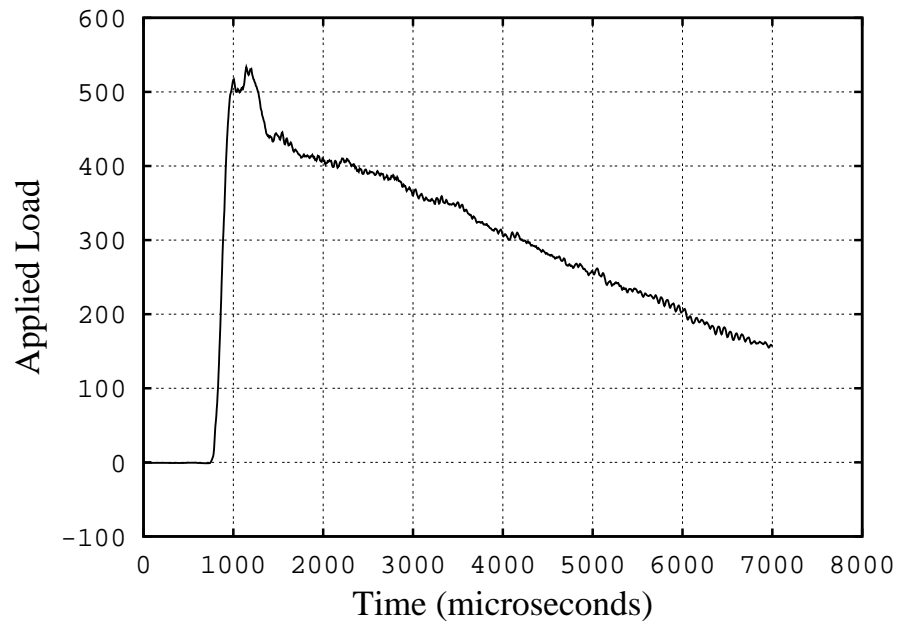Figure 3.13: Higher frequency content "True" impulse response for simulations.

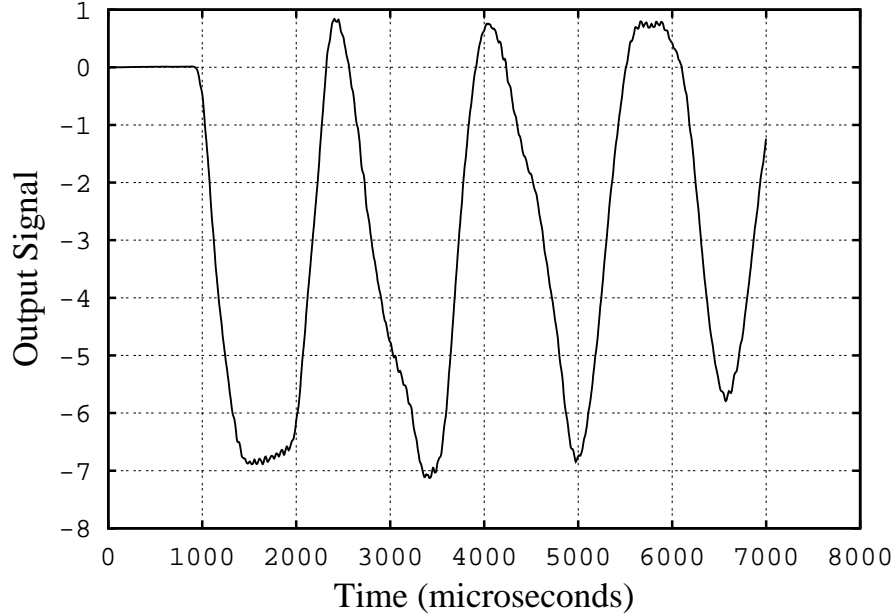Figure 3.14: Simulated tunnel applied load signal.

Figure 3.15: Simulated output signal for input of Fig. 3.14 and impulse response of Fig. 3.13.

see the effects of calibrations using pulses of different pulse duration. Simulated applied load pulses of unit impulse and of durations 50, 150 and 500 μs were convolved with the "true" impulse response, this time the one shown in Fig. 3.13. The output signals were then deconvolved with the pulse signals to infer the impulse response of the system. The simulated tunnel output signal of Fig. 3.15 was then deconvolved using each of the three inferred impulse responses, as well as the "true" impulse response. The results from this are shown in Fig. 3.16. It can be seen that all impulse responses recover the applied load well although the result for the impulse response determined from the the 500-μs pulse shows more noise than do the other cases. The time scale is expanded to show a 2 ms window of the signal in more detail in Fig. 3.17. This shows larger oscillations in the signal recovered using the impulse response from the 500 μs pulse calibration than for the other impulse responses. This can be attributed to the broader pulse not exciting high frequency in the pulse response and thus the high frequency content of the inferred impulse response is in error. Nevertheless, if the recovered, noisy force signal is passed through a 30-μs moving-average filter (that is a six-point moving-average window for the present sampling period of 5 μs), the differences between the "true" load and the recovered load are minor, see Fig. 3.18.

Thus, for implementation of force balances of the type considered here, the conclusions drawn at the end of section 3.2.1, about the suitability of calibrating a SWFB with a broad pulse, are appropriate. However, it is recommended that the frequency content of the impulse response for a system and the range of frequencies excited in a pulse test be considered carefully before applying this principle. A series of simulations, such as those reported here, would be appropriate for cases where the impulse response and pulse signals differ appreciably from those reported here.

3.2.3 Some practical limitations for calibrations using pulse inputs

There are cases where a SWFB with a high frequency response is required but the balance is also required to be operated over relatively long periods of time. This applies, for example, in balances required to measure forces on scramjet and other models in which a combustible
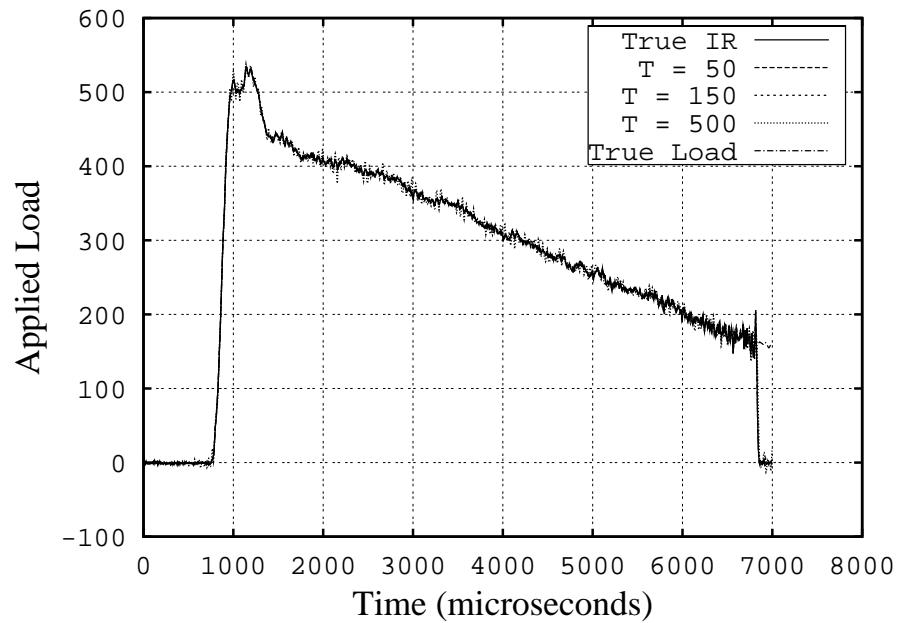
Figure 3.16: Recovered inputs for impulse responses formed from pulse responses of different pulse widths. The pulse durations shown in the legend are in microseconds.
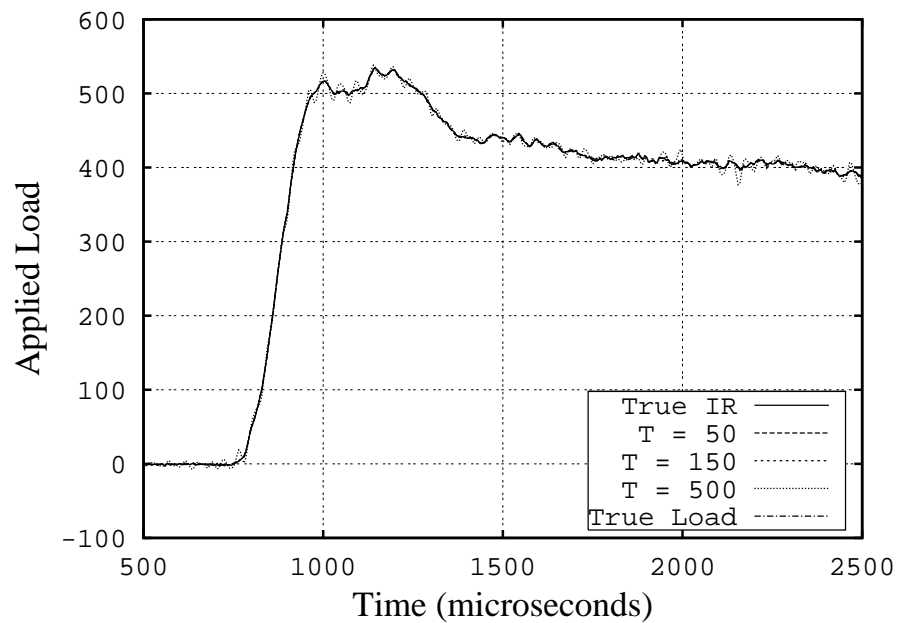

Figure 3.17: Recovered inputs for impulse responses formed from pulse responses of different pulse widths shown for 2 ms window. The pulse durations shown in the legend are in microseconds.
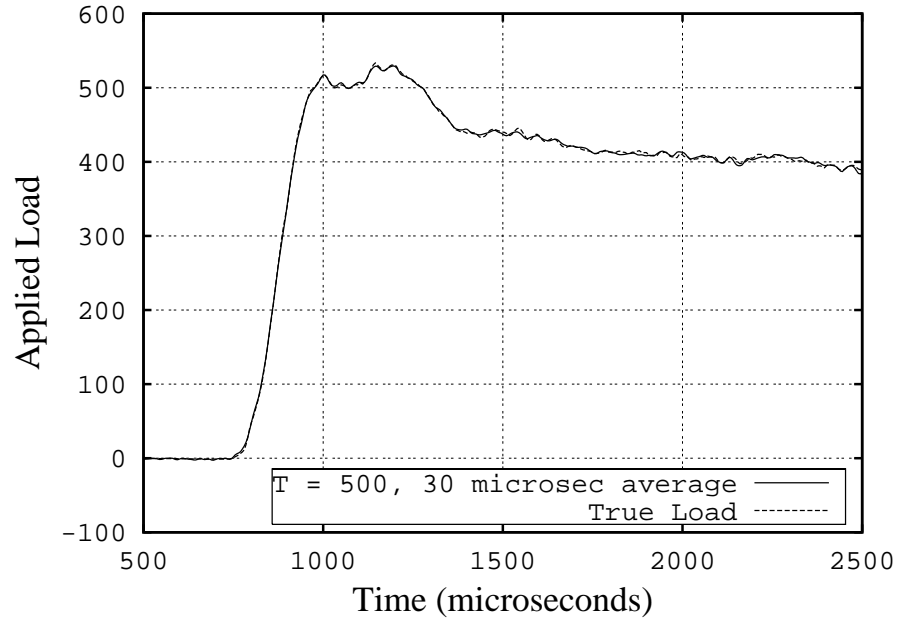
Figure 3.18: Comparison of true input and a filtered version of the recovered input for the impulse responses formed from 500 μs pulse calibration.

gas is ejected and burned (e.g. Paull *et al.*, 1995; Mee *et al.*, 2001). In the T4 shock tunnel, a fast-acting valve, triggered by the recoil of the compression tube, is used to start the flow of the injectant prior to arrival of the test flow over the model. The injectant flow is usually timed to begin several milliseconds before the test gas arrives. A solenoid valve can be required to initiate the opening of the main valve (that initiates the injected gas flow) (Morgan & Stalker, 1983) and that solenoid can be triggered 10 ms or more prior to the main valve opening fully. For some models (such as those cited above), the fuel valve is located at the end of a fuel reservoir located between the model and the stress bar. The operation of the solenoid and the main valve can apply forces to the model and balance arrangement that induce strains in the strain gauges of the balance. Also, the flow of the injectant gas can produce a thrust (and possible lift and pitching moment) on the model. Therefore, while the test period may be only 2 to 3 ms, it may be necessary to interpret the signals from the force balance for a period of the order of 15 to 20 ms. In cases such as this, the duration of the pulse in a pulse calibration may be of the order of 100 to 250 μs or about 1% of the duration for which characterization of the balance is required from the calibration.

Errors in the zero level for the pulse sensor

When a pulse is much shorter than the length of the measurement signal, small errors in the zero level of force, indicated by the pulse measurement system, can lead to large errors in the impulse response. This comes about because the total impulse provided by the impactor during a calibration is determined by the integral of the force-time signal. If the measurement system indicates a small, residual force (positive *or* negative), after the pulse, then this may integrate to a significant error in the total impulse that is applied.

To demonstrate this effect, consider the pulse of 150 μs duration that was used in the simulations of chapter 3 (see Fig. 3.7). An offset of 0.5% of the peak of the pulse is added to the signal. Both the original and offset pulse signals are shown in Fig. 3.19. While the

difference between the two signals is just large enough to see, the total impulse applied for the two force-time histories are very different. The original pulse of Fig. 3.7 had a total impulse of unity. However the offset pulse has a total impulse in excess of 140% of that of the original pulse; the long tail integrates to 42% of the impulse in the pulse itself. If now the impulse response is determined by dividing the pulse response by the area under the pulse-time curve (as investigated in section 3.2), then the impulse response will be only 70% of the correct magnitude. Strain signals deconvolved using this impulse response will give force signals that are 30% below the correct value. This error can be overcome by identifying the region of the pulse in the force-time curve and integrating that signal only over that region. For the present signals under consideration, this will produce an overestimate of the impulse of only 0.8% and forces deconvolved using an impulse response from this will be less than 1% too low.
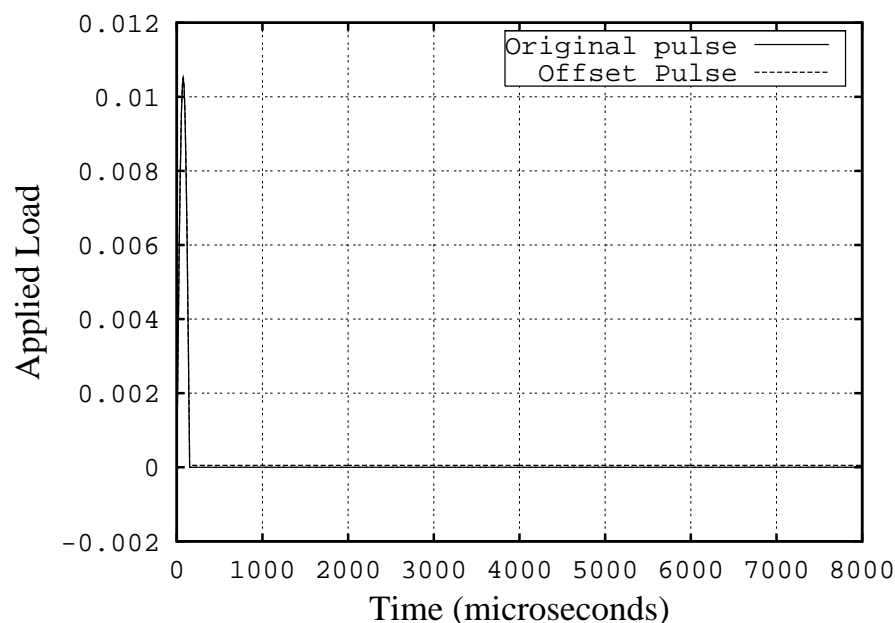

Figure 3.19: 150 μs duration pulse input with 0.5% zero offset.

What is the effect on the calculated impulse response if the output strain signal is determined using the deconvolution technique of section 3.2.1 and this "erroneous" pulse signal? Again, such an impulse response will lead to large errors but, in this case, the error will increase with time. The impulse response determined by deconvolving the output signal of Fig. 3.8 with the pulse of Fig. 3.19 is compared with the "true" impulse response in Fig. 3.20. The difference between the two impulse responses appears to be very small. However, there is a cumulative difference that leads to large errors in signals deconvolved using this impulse response. This is demonstrated by deconvolving the simulated output signal of Fig. 3.3 with the erroneous impulse response of Fig. 3.20. The result is compared with the "true" applied load in Fig. 3.21. It can be seen that the error in the recovered input continuously increases with time. If the offset in the pulse signal is a negative one, the recovered load will be increasingly lower than the load level as time increases. The bias error would be absent if the pulse signal did not have a non-zero mean after the pulse. Again the error can be eliminated by identifying the region of the applied pulse of force and setting the pulse-time signal to zero outside those times. Such a procedure will be valid for a hammer-type impact where it is known that there is no force outside of the time during which the hammer and model are in contact. This will be the case for elastic impacts provided that the hammer

does not "bounce" during the period of interest (i.e. the hammer strikes the model more than once). Such bounces can be clearly seen in the pulse signals and repeat calibration tests can be made. If there is some uncertainty about the true period of contact between the hammer and model, it can be checked (for a metallic hammer and model) by setting up a small potential difference between the hammer and model. The period of electrical short circuit can then be compared with the duration of the force pulse from the hammer signal.
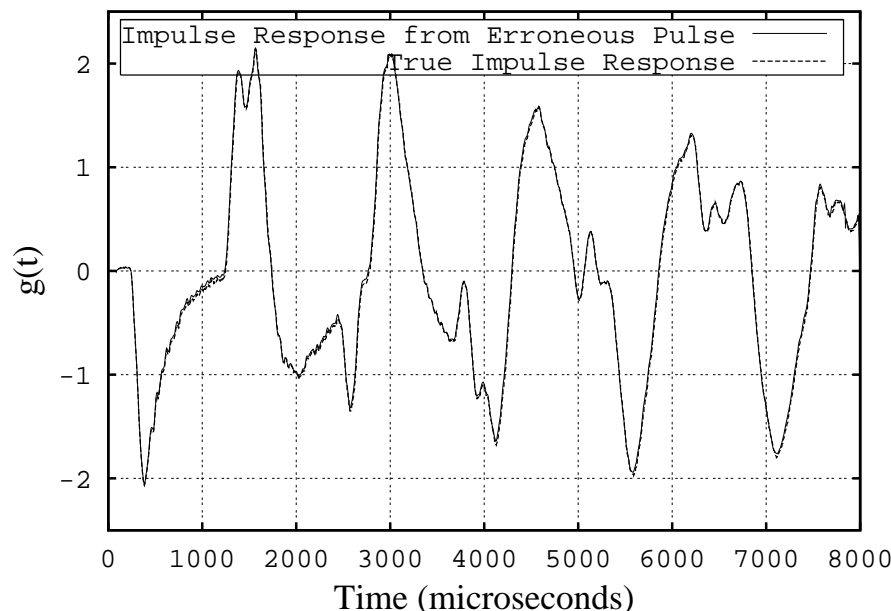

Figure 3.20: Impulse response determined by deconvolving the pulse response signal of Fig. 3.8 with the erroneous pulse of Fig. 3.19. It is compared with the "true" system impulse response.

A quick check can be made to determine whether the pulse signal is likely to suffer from these effects. A true impulse, when convolved with a step, should return a step. If the pulse signal from a pulse test is convolved with a step, the response should rise from zero and continue to rise for the duration of the pulse. It should then remain at a constant level for later times. A signal that has a positive mean after the pulse will continue to rise after the pulse and for a negative mean, the signal should fall. This is demonstrated with the original and distorted pulse signals of Fig. 3.19 in Fig. 3.22.

An example of a calibration test that is affected by an offset in the hammer signal is presented in Appendix A in section A.2.

Errors in the output signal sensor

Another potential source of error in a pulse calibration is in the measured output signal (for SWFBs, this is usually a strain signal). This error can be just as serious as a small error in the pulse signal just considered, but is potentially more difficult to detect and correct. The pulse calibration can be significantly corrupted by low frequency noise on the output signal, even when the noise is very small. A potential source of such noise is line frequency (50 Hz) noise that may be picked-up in the output measurement system. This is best illustrated with an example.

Consider again the pulse of 150 μs duration that was used in the simulations of chapter 3 (see Fig. 3.7). The signal that would be obtained when this pulse was applied to the system
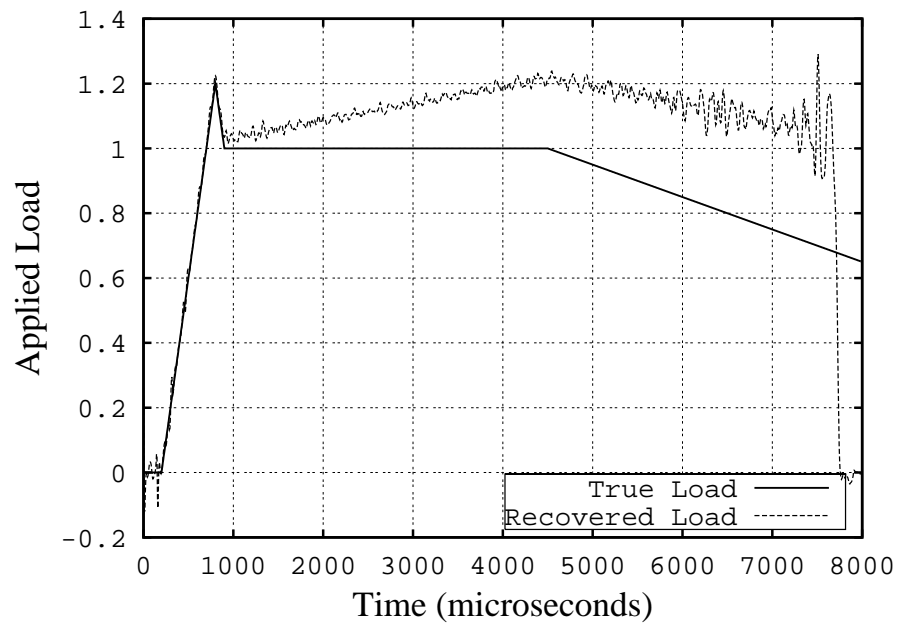
Figure 3.21: Recovered input using the erroneous impulse response compared with the true applied load.
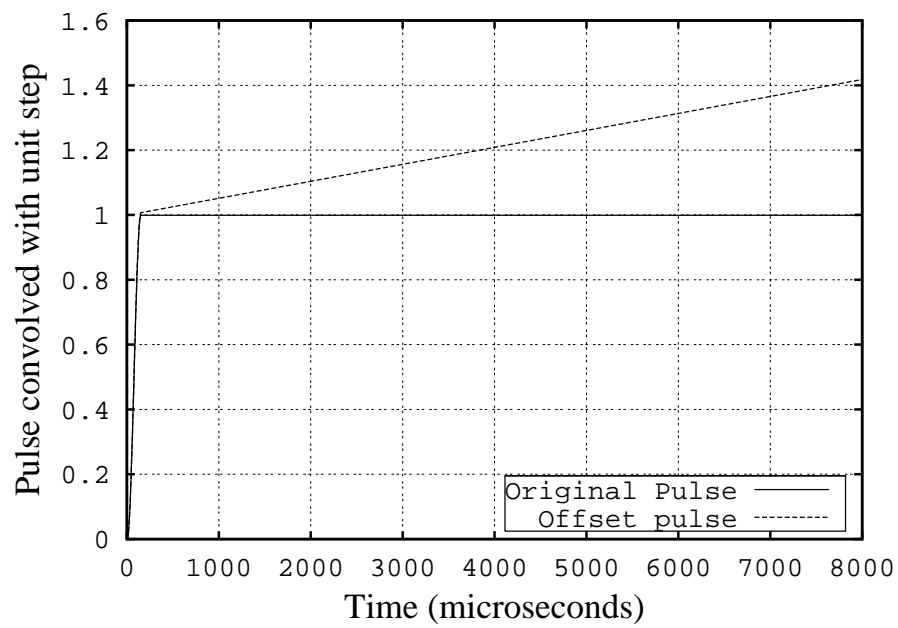

Figure 3.22: Checking the pulse signal by convolution with a step.

is shown in Fig. 3.8. Now add a small, 50 Hz noise signal to the signal detected by the output measurement system. The output signal in response to the pulse varies between approximately -2 and +2 V. Let the noise added be a sinusoid of 20 ms period and with a 40 mV peak-to-peak level. This gives a signal-to-noise ratio of approximately 100. The "true" output signal, the noise added and the "noisy" output signal are shown in Fig. 3.23. On the scale of the plot, the noise added to the output signal is almost imperceptible.

An impulse is now formed by deconvolving the "noisy" output signal with the pulse of Fig. 3.7. This impulse response is now used to deconvolve the simulated tunnel output signal of Fig. 3.3. The result is compared with the "true" applied load signal in Fig. 3.24. Again here a small error in a calibration signal used in a pulse calibration (in this case the output signal) can lead to small errors in the impulse response that result in large errors in the low-frequency components of the deconvolved input signal. The error will be similar if the impulse response is determined from the "noisy" output signal by dividing it by the area under the pulse-time curve as described in section 3.2.1. A similar error could be induced if there is some drift in the output signal (due, for example to temperature effects on strain gauges). However this is should be easily detected in the measurement system. For example, for a similar error to that seen in Fig. 3.24, a drift of about 20 mV in 8 ms would be required. This corresponds to drift rate of 2.5 V/s.
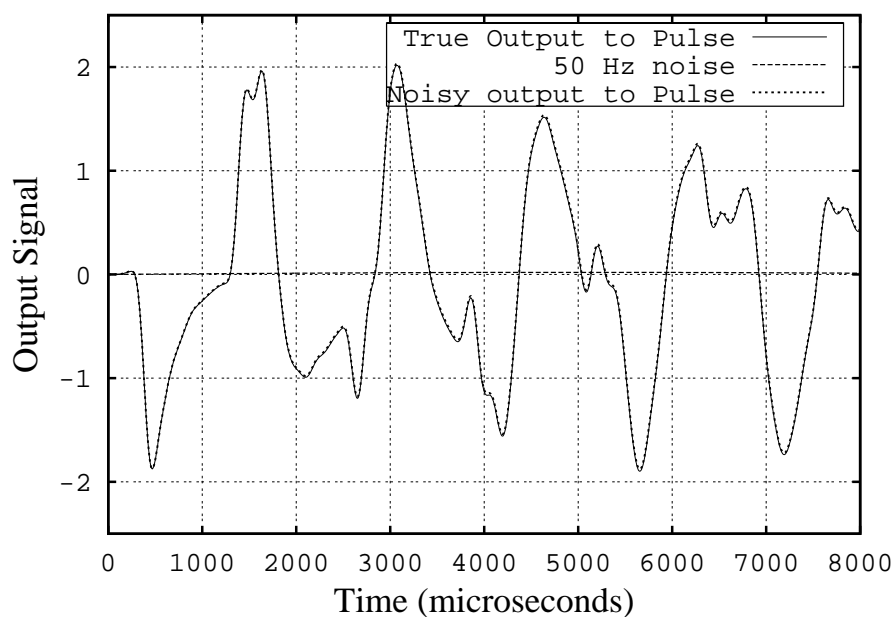

Figure 3.23: "True" output to the pulse of Fig. 3.7, the noise added to it and the addition of the two giving the "noisy" output signal.

This type of problem will arise for any source of noise with components in a frequency range similar to that for which the deconvolved input signal is required. The results here show that, even when this noise is of a low level, it can affect a pulse calibration. High frequency noise can be treated with filters (analogue or digital) and noise at frequencies much lower that that required in the deconvolved input signals will not affect the result.

An example of a calibration test that is affected by low frequency noise on the strain signal is presented in Appendix A in section A.3.

Clearly, prior to calibration, the pulse (input) and output signals should be checked for noise, in the range of frequencies required for the recovered input signals, and that noise should be minimized. However, if there remains some residual noise that can't be eliminated
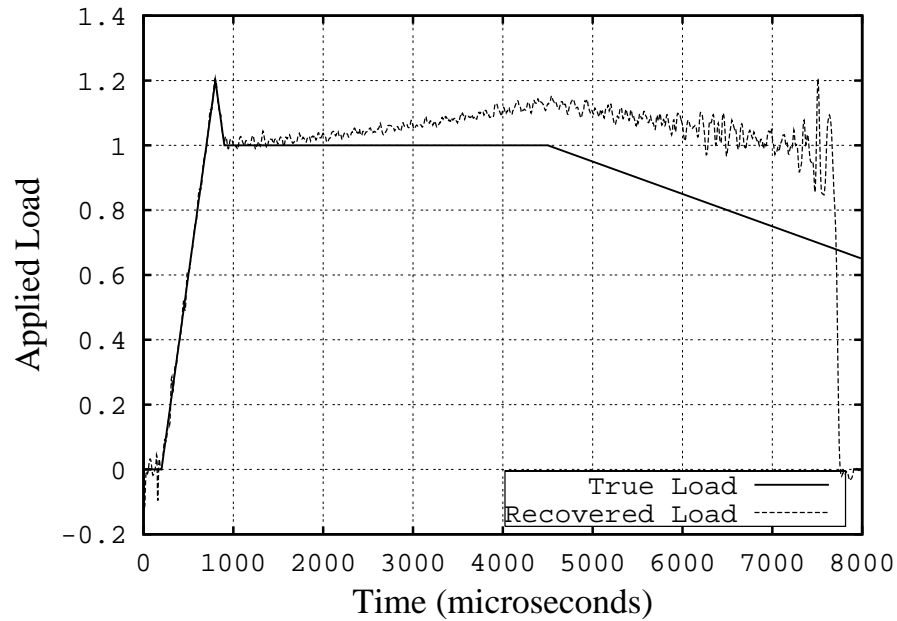
Figure 3.24: Recovered input using the impulse response corrupted by noise on the pulse output signal compared with the true applied load.

from either signal, the following are recommended. If there is low frequency noise in the pulse signal, the period of time when the pulse input is applied to the system should be identified and the signal set to zero at other times. If there is low frequency noise in the system output signal, the output signal should be recorded for an appropriate period of time prior to the pulse input the the system. Then any noise at problem frequencies (particularly line frequency) may be able to be characterized (amplitude, wave shape and phase) and numerically removed from the output signal prior to determining the impulse response. The period of time required for such characterization will depend upon the frequency of the noise and the period for which the impulse response is required.

Chapter 4

Experiments

4.1 Model and force balance

In order to check the theory and simulations presented in chapters 2 and 3 for a physical balance and to demonstrate some of the issues raised, a simple single-component stress wave force balance has been used in bench tests and in flow tests in the T4 shock tunnel at The University of Queensland.

The model used was a 15°-semiangle sharp cone of 182 mm axial length. The body of the cone was made from aluminium and it had an 18 mm long stainless steel tip. The cone was mounted on a tubular brass stress bar of 2.4 m length, 32 mm outer diameter and 1.7 mm wall thickness. For the pulse calibration tests and the tunnel tests, the complete model was suspended by two fine wires, as in Fig. 2.1. There were two steel tips for the model; one sharp and the other a cylindrical tip of 13 mm diameter and 25 mm length with a flat end. The cylindrical tip was used to apply loads in the calibration tests. For the calibration tests in which either the model was suspended on a fine wire or a weight was attached to the model via a wire (see Fig. 2.3), the cylindrical tip was used. To attach the wires a hole of 1 mm diameter and 15 mm depth was drilled into the end of the tip down the axis of the model. A hole for an M3 grub screw was made into the side of the tip, 10 mm from the end, so that a wire could be inserted into the 1 mm hole and secured via the grub screw. For the pulse tests, the impactor was used to strike the model on the flat end of the cylindrical tip.

Piezo film (polyvinylidine fluoride or PVDF) was used as a strain sensor (Smith & Mee, 1996b). The gauge used in the tests was labelled *PF3* and was a 25 mm long piece of piezo film wrapped around the stress bar with its most sensitive axis aligned with the axis of the bar. Such an arrangement provides bending compensation so that only axial strains are measured (Smith & Mee, 1996b). Gauge *PF3* was located 425 mm from the junction between the model and the stress bar. The gauge was connected to a PCB Charge Amplifier that had a frequency response of 0.3 Hz to 180 kHz at -3 dB break points. In all tests a data-acquisition system was used to sample the signals at 5-μs intervals.

In the tunnel tests, the model and stress bar were aligned with the flow so that only axial aerodynamic loads were present and the complete arrangement was free to move in the axial direction. The base of the cone was shielded from the flow to minimize any contribution of base pressure to the force on the cone. The shielding surrounds both the sting and the support threads, to protect them from experiencing any aerodynamic loads, as shown in Fig. 2.1. During the flow time the model was able to move freely in the axial direction without touching the shielding. In the tunnel shots the Pitot pressure in the test section was measured simultaneously with the drag force measurements. The Pitot probe was set in line with the base of the cone but 75 mm from the axis of the cone. This meant that

the Pitot probe was within the test core of the nozzle but was outside of the shock from the cone. Also, at that location, the bow shock from the probe does not strike the cone.

4.2   Bench tests

The bench tests involved three of the calibration techniques discussed in chapters 2 and 3; the two vertical calibration arrangements shown in Fig. 2.3, referred to as "hung-weight" calibrations (Fig. 2.3(a)) and "self-weight" calibrations (Fig. 2.3(b)), and pulse test calibrations, using the arrangement shown in Fig. 2.4. The vertical calibration tests were done prior to testing the model in the T4 shock tunnel and the pulse calibration tests were done after the shock tunnel tests, but while the model was still installed in the test section of the tunnel. The calibration tests are first described and typical results from each of the calibration techniques are shown. Then cross checks are performed by deconvolving signals from one type of calibration test with impulse responses determined from the other calibration techniques.

4.2.1   Determination of the impulse response from a step response

Hung-weight test

For the hung-weight tests, the force balance/model arrangement was suspended from the downstream end of the stress bar via a loop of steel wire that passed through holes drilled through the stress bar 15 mm from its end. This wire loop was then attached to a steel frame mounted from the wall of the laboratory. The arrangement is shown schematically in Fig. 2.3(a). A mass of 4.23 ± 0.01 kg was suspended from the tip of the cone using stainless steel gauge 30 wire (0.3 mm diameter). This wire was cut within 10 mm of the tip of the model using standard, sharp wire cutters.

A sample step response obtained from such a test, test HW112, is shown in Fig. 4.1. It can be seen that the output signal is initially at the zero level and that there is a sudden change in the output signal at time ≈ 500 μs. In order to obtain this result, the data acquisition system was triggered using the sudden change in the level of the strain signal with a fixed number of pre-trigger samples. The actual time at which the load was removed from the tip is not time zero in the figure. However, this time can be estimated by considering the propagation of stress waves between the points of application of the load and measurement of the strain. This requires knowledge of the distance to the strain gauge from the tip of the model and the material of the structure between the tip and the gauge. For the present model, the first 25 mm of the stress wave's path is through the steel tip of the model, the next 164 mm through the aluminium model and the final 425 mm through the brass stress bar. Taking the stress wave speeds in these three materials to be 5.2, 5.0 and 3.5 km/s respectively, the time taken for the first waves to reach the gauge will be approximately 160 μs. Thus, for this case, the cut time is at approximately time 340 μs in Fig. 4.1.

The impulse response can be determined by differentiating this step response with respect to time, as described in section 2. To get the timing correct, the signal must first be shifted in time, in this case by -340 μs, and differentiating the resulting signal. This time shifting is done to account for the somewhat arbitrary triggering time of the data acquisition and for the delay between forces being applied to the model and stress waves due to those forces reaching the strain gauges on the stress bar. Since the calibration load in this case is applied at the tip of the model, the time delay due to stress wave propagation is 160 μs as calculated above. This value is appropriate for the present situation where the loading is due to a point

load applied at the tip of the model. When an impulse response is required for deconvolving signals from a test in a wind tunnel, it could be argued that this time delay may not be appropriate. Aerodynamic forces will be distributed over the surface of the model an will not be concentrated at the tip. Thus when using an impulse response such as that determined from an hung-weight test, it may be more suitable to determine the delay in wave propagation for some other reference point on the model. This will become more important as the model size increases. This also raises the question of the sensitivity of the performance of the force balance to the way in which the forces are distributed over the model. This question is addressed in Tuttle *et al.* (1995).
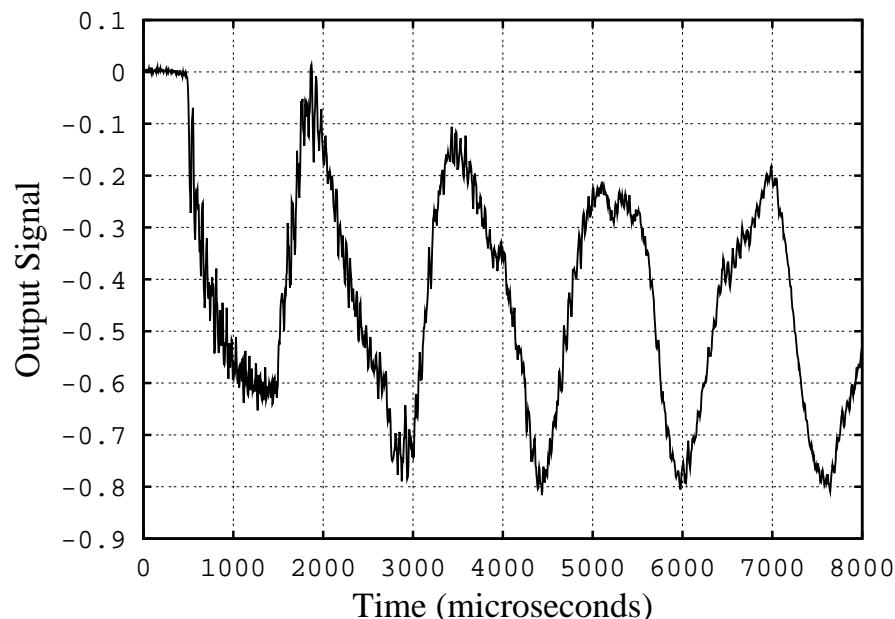

Figure 4.1: Sample step response obtained by cutting a wire supporting a mass suspended from the tip of the model (Hung-weight test HW112).

Self-weight test

for the self-weight tests, the force balance/model arrangement was suspended from the tip of the model using stainless steel gauge 30 wire as shown in Fig. 2.3(b). The wire was cut within 10 mm of the tip of the model using wire cutters. The total mass of the model, force balance and cables being suspended by the wire was 4.94 ± 0.02 kg. A sample result from such a self-weight test, test SW202, is shown in Fig. 4.2. As for the hung-weight test, the output signal is initially at the zero level and drops suddenly when the first stress waves reach the gauge location. There are two obvious differences between the signals in Figs. 4.1 and 4.2. Firstly, the level of the signal for the self-weight test is higher than that for the hung-weight test between times 500 and 1500 μs. This can be attributed to the different load levels being removed - the weight of a 4.94 kg mass compared with that of a 4.23 kg mass. The second difference occurs after the waves that have reflected from the downstream end of the stress bar reach the gauge measurement location (at time approximately 1500 μs in Fig. 4.2). Note that the relative depth of the second trough compared with the first is more for the hung-weight test. As will be discussed in section 4.2.3, this is associated with the difference in the support condition at the end of the stress bar. It may also be noted that the change in the output signal is "sharper" for the self-weight test in Fig. 4.2 than it
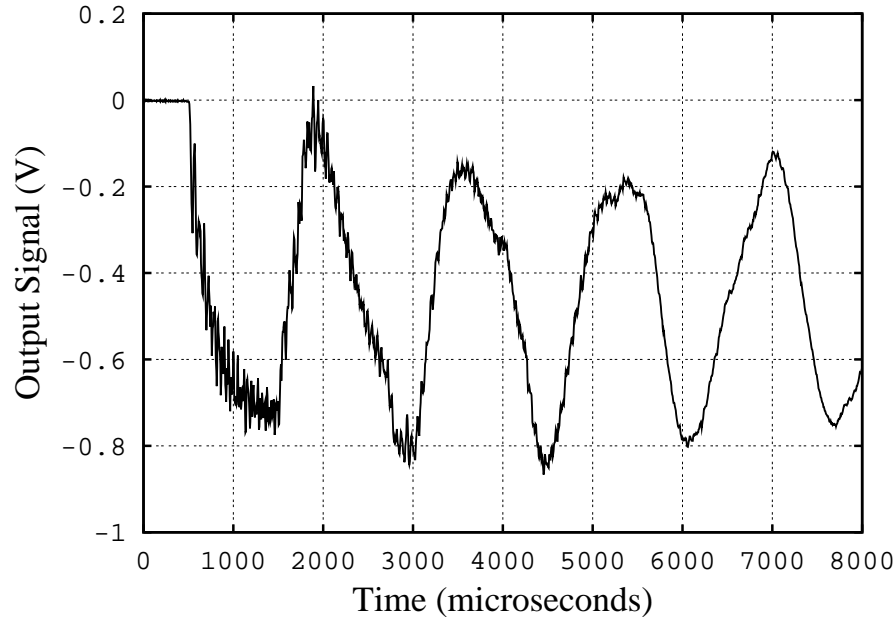
32

Figure 4.2: Sample step response obtained by cutting a wire supporting the model vertically from its tip. (Self-weight test SW202)

is for the hung-weight test in Fig. 4.1. The significance of this is also discussed further in section 4.2.3.

As for the hung-weight test, the the time at which the wire was cut was determined by estimating the time for stress waves to travel from the tip of the model to the strain gauge location. The impulse response can be determined from this step response by shifting the signal in time, again in this case by about -340 μs, and differentiating the resulting signal with respect to time. The impulse response is similar to that shown in Fig. 3.13.

4.2.2 Determination of the impulse response from a pulse response

The pulse calibration tests were done while the model was still installed in the test section of the T4 shock tunnel. The calibration tip was attached to the end of the cone in place of the sharp tip that had been used in the tunnel shots. The arrangement of the model and its suspension in the tunnel is shown schematically in Fig. 2.1. A PCB model 086C04 impulse force hammer was used to apply and measure the force pulse. The hammer uses a PCB ICP to condition the signal. The hammer was equipped with a steel tip. No extender was used.

A sample force pulse applied with the hammer in a pulse calibration test, test 6274H7, is shown in Fig. 4.3. The region of the force pulse is shown in more detail in Fig. 4.4. It can be seen that the pulse is of about 240-μs duration and is approximately symmetrical in shape. There is some ringing of the transducer after the pulse and this decays to zero after about 1 ms. This ringing was larger in some pulse tests but the oscillations usually had a zero mean. The corresponding strain output signal from sensor *PF3* is shown in Fig. 4.5.

The hammer signal can be checked using the method outlined in section 3.2.3 by convolving the pulse with a unit step. The result is shown in Fig. 4.6. It can be seen that the check signal is almost flat after the end of the pulse. A "modified" hammer signal was also prepared for this test; the hammer pulse was identified to occur between times 90 and 330 μs in the plot of Fig. 4.4 and the signal was set to zero at other times. The result obtained

33

when this modified signal is convolved with a unit step is also shown in Fig. 4.6. In this case, there is little difference between the raw and modified hammer signals.
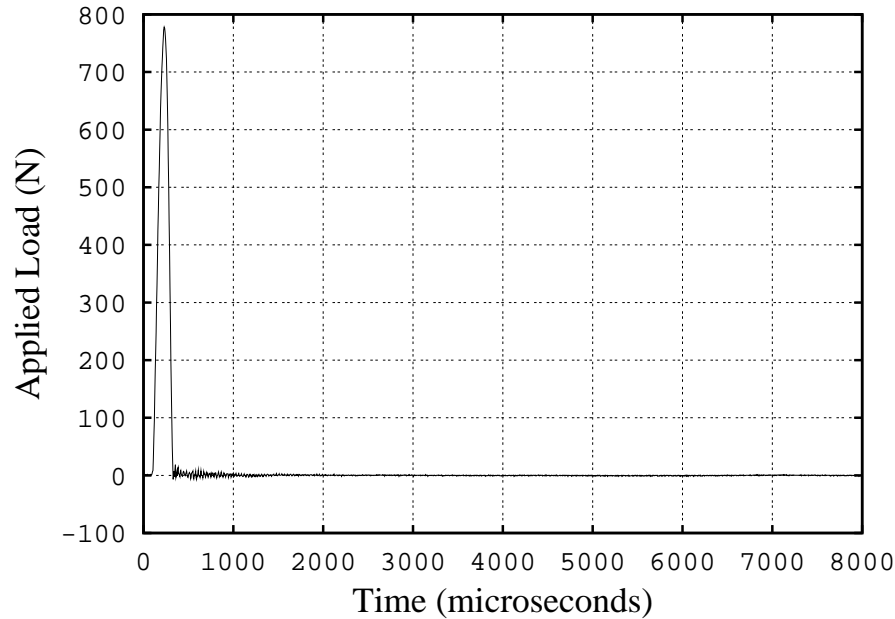

Figure 4.3: Sample force pulse applied at the tip of the cone with the impulse force hammer (test 6274H7).

From the output signal of Fig. 4.5 and the hammer pulse of Fig. 4.3 the impulse response of the system can be determined using the two methods outlined in section 2.2. To determine the impulse response by dividing the pulse response by the impulse applied by the hammer, the area under the force *vs* time curve for the hammer pulse must be determined. This has been done for the pulse of Fig. 4.3 and the total impulse applied over the 8 ms window is 0.102 Ns. The value obtained for the modified pulse is 0.101 Ns, indicating that there is little error in the mean level of the hammer pulse signal after the pulse (as can be inferred visually from Fig. 4.6). Note that this is not always the case. The impulse response has also been determined by deconvolving the output signal of Fig. 4.5 with the modified hammer pulse signal. The results are discussed in section 4.2.3.

4.2.3   Cross-checks on calibration techniques

Six impulse response functions have been determined from the sample calibration tests. These impulse responses are numbered IR 1 to IR 6 and are formed from

1. the hung-weight test, HW112,

2. the self weight test, SW202,

3. the hammer pulse test, 6274H7, by dividing the measured response by the area under the force *vs* time curve using the raw hammer signal,

4. the hammer pulse test, 6274H7, by dividing the measured response by the area under the force *vs* time curve using the modified hammer signal,

5. the hammer pulse test, 6274H7, by deconvolving the measured response with the raw hammer signal, and
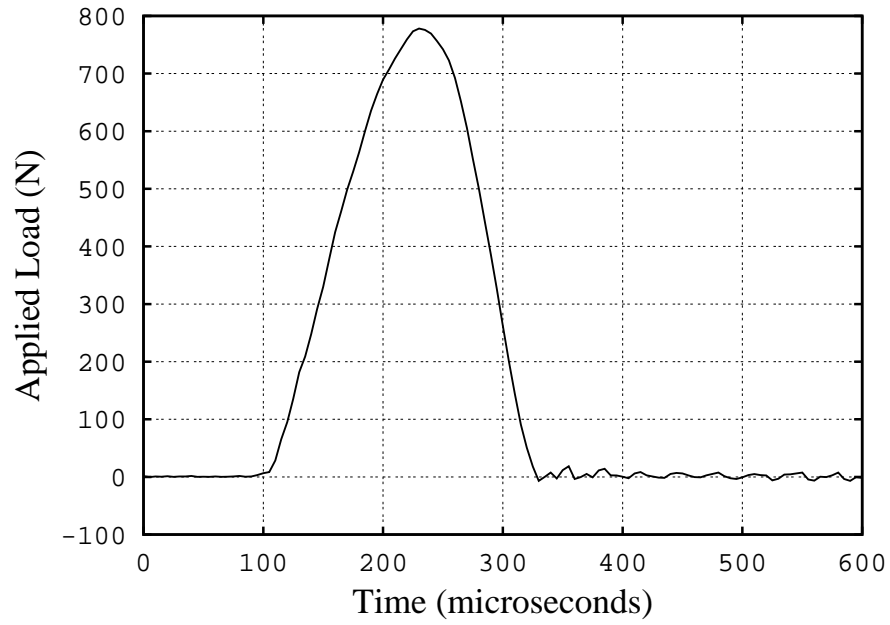
34

Figure 4.4: The sample force pulse of Fig. 4.3 shown in more detail (test 6274H7).
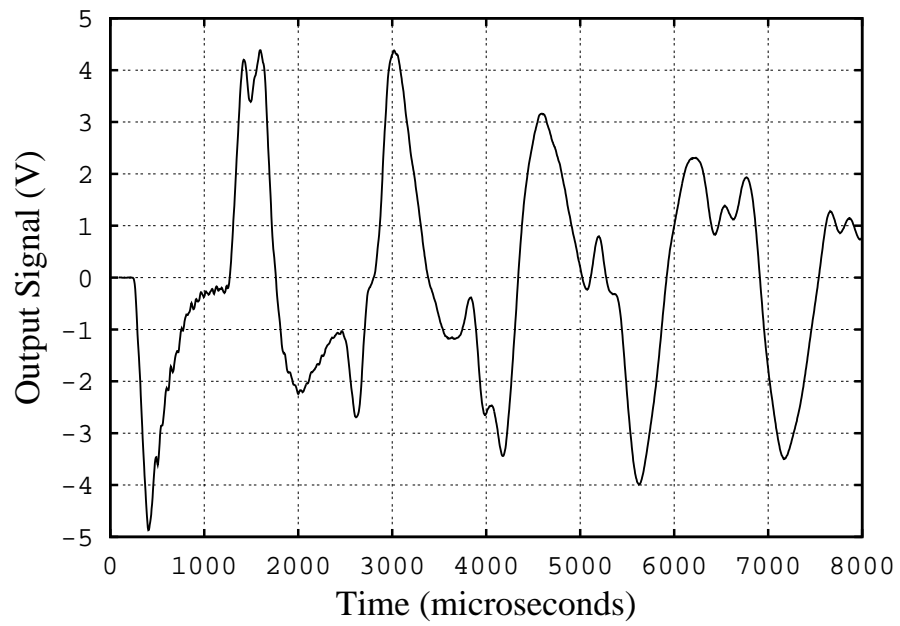

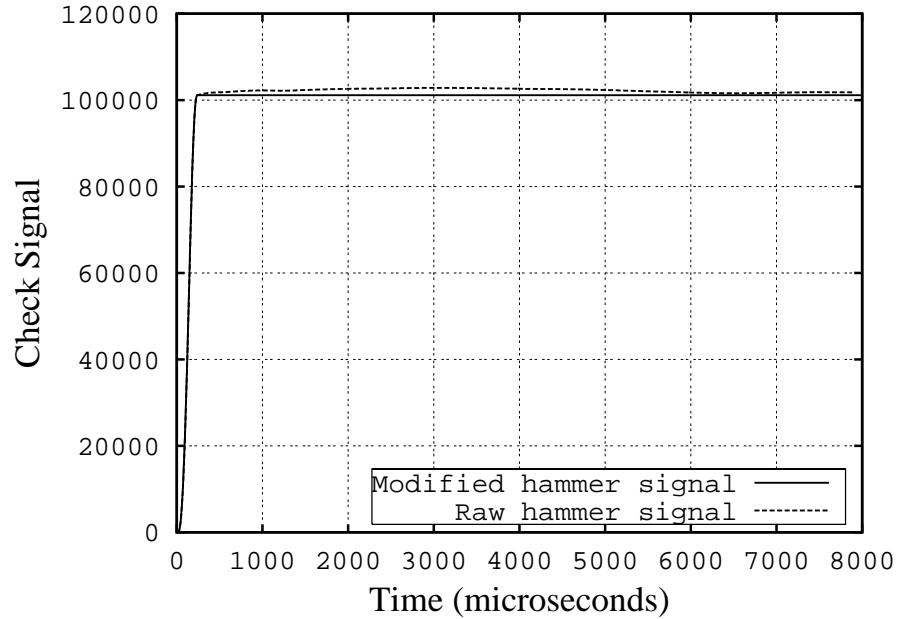Figure 4.5: Response of balance to the force pulse of Fig. 4.3.

Figure 4.6: Check on the force pulse of Fig. 4.3 by convolving the pulse signal with a unit step. Shown also is the check for the modified hammer signal (the signal set to zero outside region of the pulse).

6. the hammer pulse test, 6274H7, by deconvolving the measured response with the modified hammer signal.

In determining the impulse responses and using them for deconvolution, it is appropriate to consider the effects of noise on the results and appropriate filtering of the signals. As noted, a 200 kHz sampling frequency (a 5-μs sampling rate) was used for the data acquisition system for the impulse response calibration tests and and for recording the shock tunnel results. For the type of signals expected in the shock tunnel tests, information up to frequencies of approximately 30 kHz is expected to be sufficient. There are many different types of filters that could be used to filter out higher frequency noise. Moving-average filters, that are simple to implement and use, have been found to be adequate for filtering the type of signals obtained using stress wave force balances. For these present tests, a 30-μs moving-average filter (a six-point filter for the current sampling rate) has been chosen.

In order to determine impulse responses 1, 2, 5 and 6, the measured strain signals were first processed with a 30-μs moving-average filter. As discussed in section 3.2, the impulse responses for cases 3 and 4 will have a frequency response set by the duration of the pulse applied. Using these impulse responses, it would not be possible to obtain information about frequencies as high as 30 kHz. So a longer-duration moving-average filter is necessary for these impulse responses. Testing indicates that a moving-average filter of length about half the duration of the pulse is appropriate for the impulse responses determined by dividing the pulse response signal by the impulse of the impact. To determine impulse responses 3 and 4, a 120-μs moving-average filter has been used.

These six impulse responses have then been used to deconvolve the step response obtained from self-weight test SW203. The response from a self-weight test has been chosen as the test file for deconvolution because it has the same, free-end condition at the downstream end of the stress bar as in the shock tunnel shots. Also, as is confirmed by deconvolution with impulse response number 6 above, the rise time for the step is short.

The results from the six deconvolutions are presented in Fig. 4.7. These results were obtained using the deconvolution feature in Hyforce version 1.31 with 100 iterations. The deconvolved signals obtained using impulse responses 1, 2, 5 and 6 were then processed with a 30-μs moving-average filter and those for impulse responses 3 and 4 were processed with a 120-μs moving-average filter. The timescale has been adjusted so that the weight is cut at time zero.

The result for the impulse response derived from the hung-weight test, Fig. 4.7(a), shows the effect of the wrong end condition at the downstream end of the stress bar. The recovered load is at approximately the correct level (48.4 N) for just over one millisecond after the wire was cut but then it starts to deviate from the correct value. The signal should be correct until the first reflection of stress waves from the downstream end of the bar reach the strain measurement location; until that time there can be no effect of the end condition on the result. For the present arrangement this time is estimated to be 1.3 ms, using the wave speeds in the materials of the model and stress bar. This time agrees well with the deviation from the correct load in the figure. As there are further reflections up and down the force balance, the deconvolved signal continues to deviate from the correct load value.

The result for the impulse response derived from another self-weight test presented in Fig. 4.7(b) shows a good recovery of the applied load. Towards the end of the record, the recovered signal is approximately 2% lower than the true level. The signal rise time (10 - 90%) is approximately 30 μs. This corresponds to the duration of the moving-average filter that was applied to minimize noise.

The best recovery of the load for the impulse responses determined from the pulse calibration test is for case IR 6, where the impulse response was found by deconvolving the measured strain signal with the modified hammer pulse signal, Fig. 4.7(f). Two important points are drawn from this result. Firstly, the signal level is recovered well over the entire period considered, indicating that it is possible to obtain a good estimate of the impulse response by using this pulse calibration technique. Secondly, the recovered signal is seen to rise rapidly to the correct level, indicating that the method of obtaining a step response by cutting a fine wire attaching a load to the model gives a rapid removal of the load. The is illustrated more clearly in Fig. 4.8 where the first 100 μs of this signal either side of the cut is shown. There is some noise on the signal, but it can be seen that it rises within approximately the 30 μs that was used for the moving-average filter. It can also be seen that there is about a 15-μs delay in the signal, indicating that the estimate of the time taken for waves to traverse from the tip of the cone to the strain measurement is overestimated by about 10%. So both the self-weight and the pulse calibration techniques are suitable for obtaining the impulse response for a system such as that used here.

A reasonable recovery of the step is obtained using the impulse responses determined by dividing the pulse response by the applied impulse. The expected drop in response time of the balance is apparent and there is some ringing either side of the step. There is also some ringing induced at about 1.3 ms after the step that is attributed to rapid changes in the signal level as the primary reflection of the stress waves due to the applied load return to the gauge location after reflecting from the downstream end of the stress bar. Despite some loss in frequency response, the load level is well recovered.

While there is little difference between the results obtained in Fig. 4.7 when either the raw or the modified hammer pulse signal is used to determine the impulse response, there is a small improvement in the signal in Figs. 4.7(d) and (f) when the modified pulse is used over that in Figs. 4.7(c) and (e) when the raw pulse signal is used. These differences are larger when the pulse check signal, such as that in Fig. 4.6, is not as flat after the pulse. The modified hammer pulse should be used for most accurate recovery of the applied load.
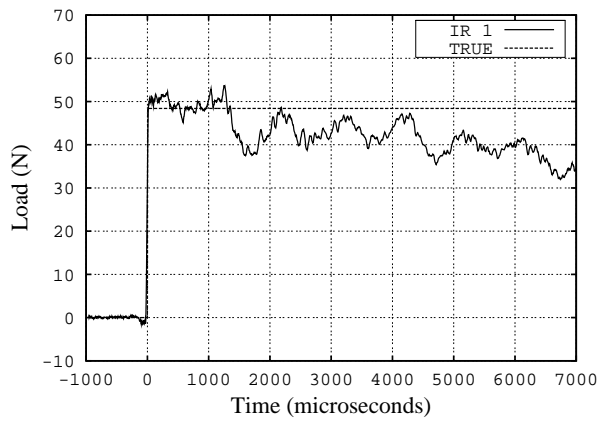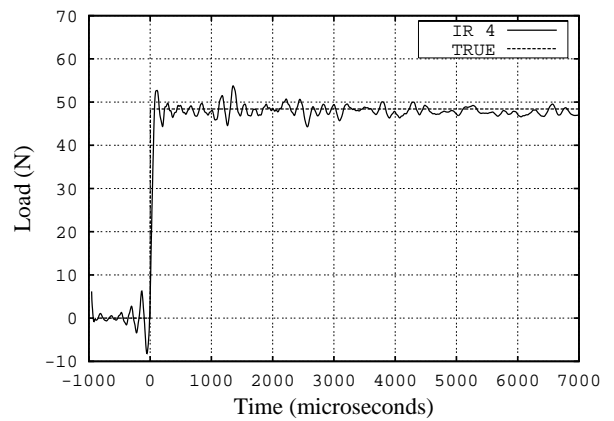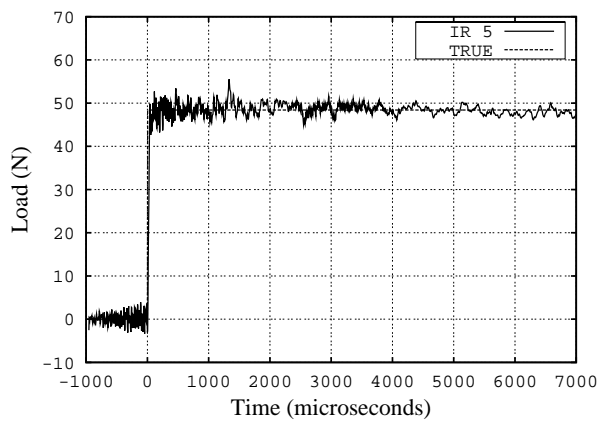
(a) IR 1, from HW112.
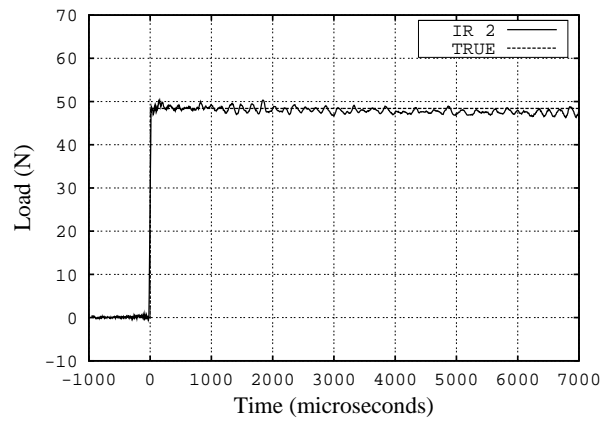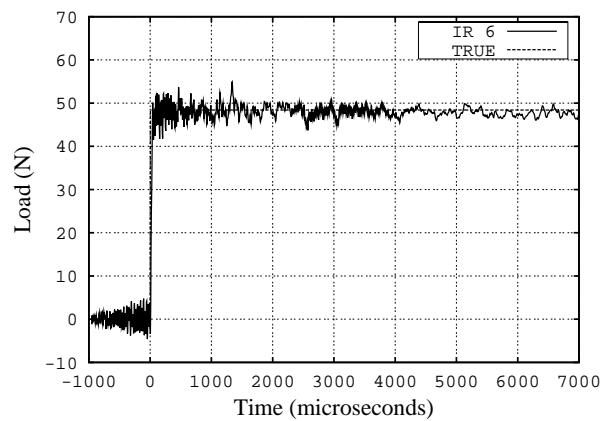
(b) IR 2, from SW202.
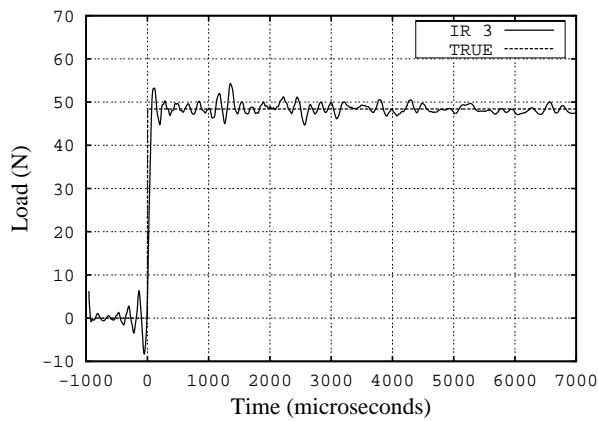
(c) IR 3, from 6274H7, area method, raw pulse.

(d) IR 4, from 6274H7, area method, modified pulse.

(e) IR 5, from 6274H7, deconvolution method, raw pulse.

(f) IR 6, from 6274H7, deconvolution method, modified pulse.

Figure 4.7: Step response of test SW203 deconvolved with the six impulse responses (100 iterations then 30- or 120-μs moving-average filter).
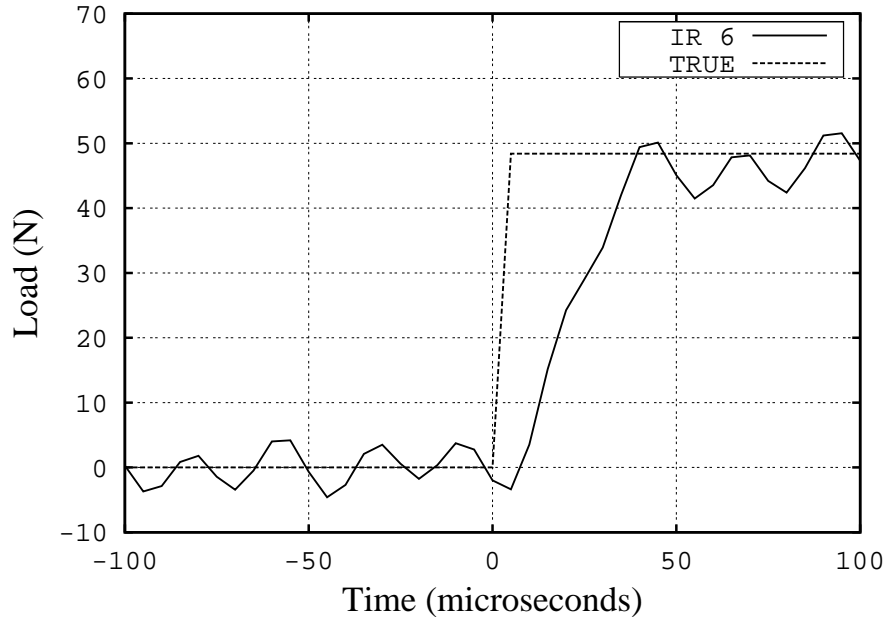
Figure 4.8: The first 100 μs either side of the cut for the result in Fig. 4.7(f).

4.3 Shock-tunnel tests

The model used in the bench tests was tested at four conditions in the T4 shock tunnel. The filling pressures and gases for the tests are shown in Table 4.1. The conditions in the nozzle supply region were determined from the shock tube filling conditions and the measured shock speed using the code ESTC (McIntosh, 1968). The measured shock speed and the derived nozzle supply conditions are shown in Table 4.2. The conditions in the test section of the tunnel were determined using the nozzle supply conditions and the nozzle shape using the code NENZF (Lordi *et al.*, 1966). The flow was expanded until the ratio of Pitot pressure to nozzle supply pressure, predicted by NENZF, matched the mean value during the test period of the measured ratio Pitot pressure to nozzle supply pressure. For shot 6271, NENZF was run in the mode where equilibrium chemistry was used in the nozzle expansion. For the other cases, non-equilibrium chemistry was used. The results are shown in Table 4.3.

Table 4.1: Filling pressures and gases for the T4 tests.

Shot	p_{res}	p_{CT}	CT gas	Diaphragm	p_{ST}	ST gas	Nozzle
	MPa	kPa		mm mild steel	kPa		
6271	4.4	53.6	100% Ar	4	200	Air	Mach 6
6272	0.72	13.7	20% Ar, 80% He	1	7.0	Air	Mach 6
6273	4.4	53.6	15% Ar, 85% He	4	50	Air	Mach 6
6274	4.4	53.6	40% Ar, 60% He	4	120	Air	Mach 6

The strain signal measured for shot 6271 is shown in Fig. 4.9. This strain signal has been deconvolved with each of the six impulse responses determined from the calibration tests in section 4.2.3. 100 iterations were used for deconvolution for each case. Prior to deconvolution, the strain signal was filtered with a 30-μs moving-average filter for the cases where IR 1, IR 2, IR 5 and IR 6 were used. For the impulse responses determined by dividing the pulse response by the magnitude of the impulse (IR 3 and IR 4), the strain

39

Table 4.2: Shock tube and nozzle supply conditions for the T4 tests.

Shot	shock speed	h_s	p_s
	m/s	MJ/kg	MPa
6271	1850	3.4	28
6272	3080	9.7	4.7
6273	3390	11.1	31
6274	2440	8.2	32

Table 4.3: Flow conditions in the test section for the T4 tests.

Shot	NENZF mode	p_{Pit}/p_s	M_∞	v_∞	p_∞	ρ_∞	T_∞	γ
				m/s	kPa	kg/m^3	K	
6271	equilibrium	0.0128	6.5	2470	6.6	0.064	360	1.4
6272	non-equilibrium	0.0130	5.9	3760	1.4	0.0046	970	1.37
6273	non-equilibrium	0.0135	5.4	4110	11.6	0.026	1480	1.33
6274	non-equilibrium	0.0130	5.7	3650	10.1	0.033	1050	1.34

signal was passed through a 120-μs moving-average filter prior to deconvolution, as discussed in section 4.2.3. After deconvolution, the same length moving-average filters were passed through the data and the final results are shown in Fig. 4.10.
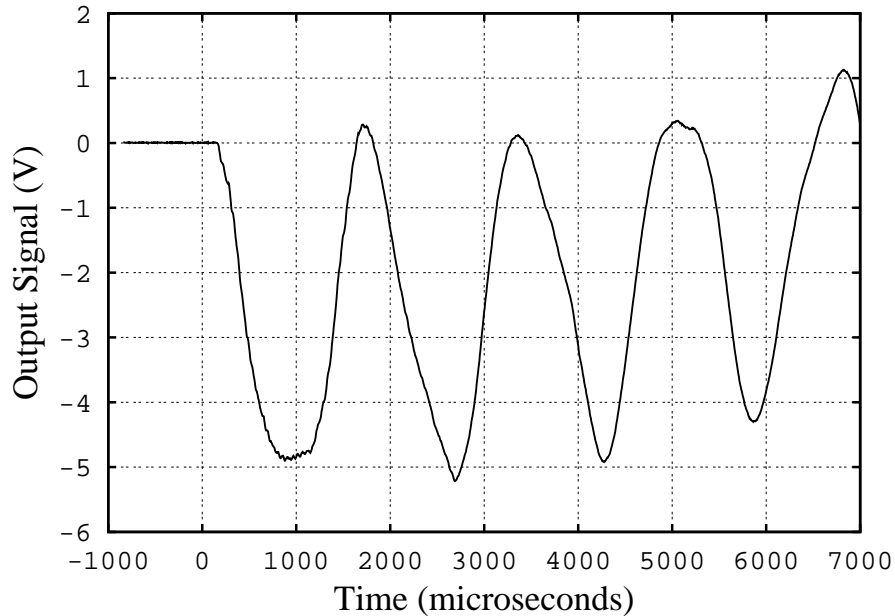

Figure 4.9: Strain signal from sensor *PF3* for shot 6271.

There are some expected similarities between the deconvolved drag signals in Fig. 4.10 and the signals from the step response test presented in Fig. 4.7. The force signal for shot 6271 determined using the impulse response that was obtained from the hung-weight test (IR 1) shows large, low frequency oscillations beyond about 1.3 ms after flow arrival. This again is attributed to the different end condition between the calibration test and the tunnel shot. The signals in Fig. 4.7(c) and (d) have small oscillations that are again attributed to the poorer frequency response associated with the calibration method used. However, the
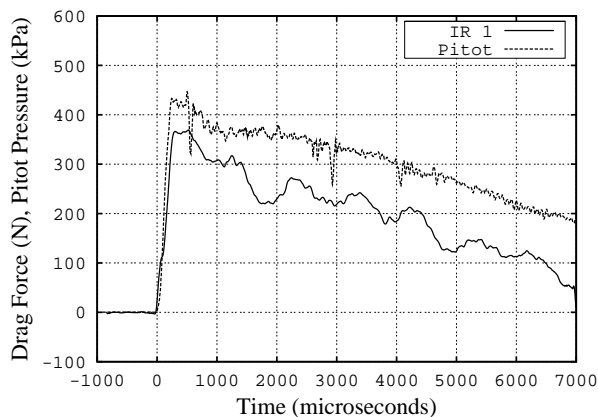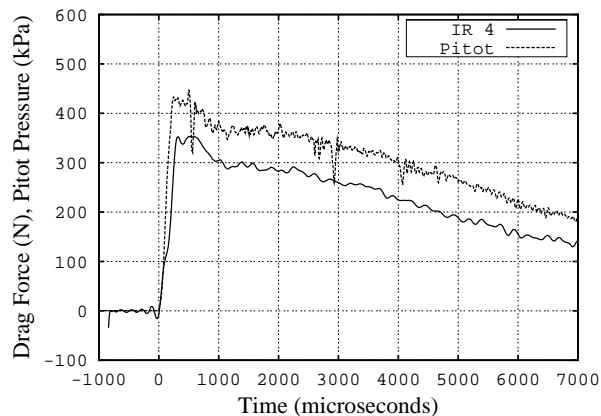
(a) IR 1, from HW112.
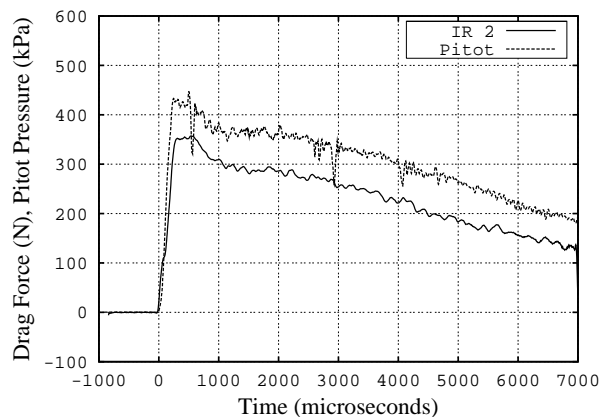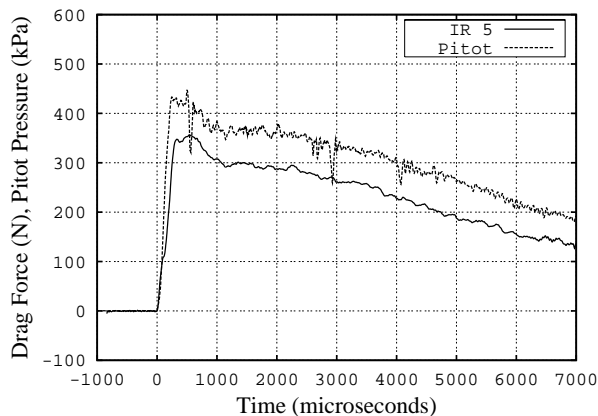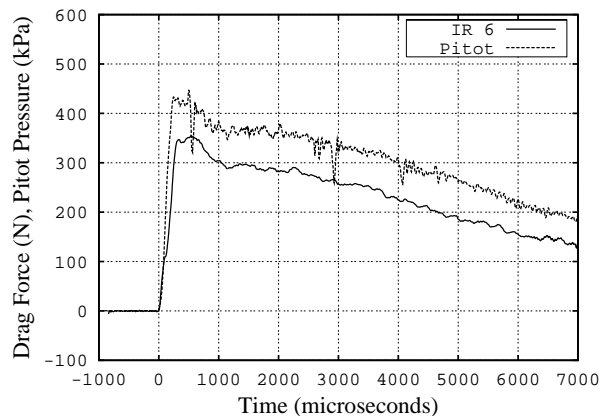
(b) IR 2, from SW202.
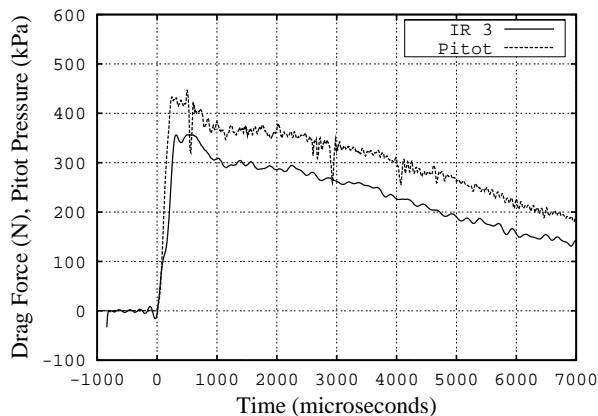
(c) IR 3, from 6274H7, area method, raw pulse.

(d) IR 4, from 6274H7, area method, modified pulse.

(e) IR 5, from 6274H7, deconvolution method, raw pulse.

(f) IR 6, from 6274H7, deconvolution method, modified pulse.

Figure 4.10: The strain signal of shot 6271 deconvolved with the six impulse responses (100 iterations then 30- or 120-μs moving-average filter).

oscillations are much smaller than for the case of the step response results in Fig. 4.7(c) and (d).

The three calibration techniques recommended for deconvolving tunnel signals such as that for shot 6271 are the self weight test (IR 2), the pulse test with the impulse response found by dividing the response by the area under the modified pulse (IR 4) and the pulse test with the impulse response found by deconvolving the response with the pulse signal (IR6). The results of deconvolving shot 6271 with these three impulse responses are compared directly in Fig. 4.11. Very good agreement between the three signals is obtained over the entire record shown.
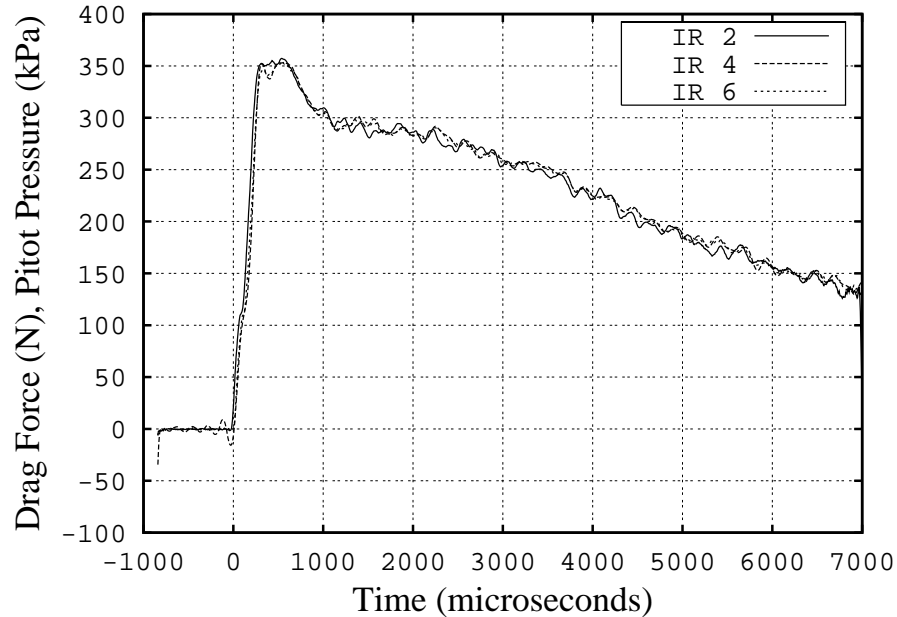

Figure 4.11: The strain signal of shot 6271 deconvolved with IR 2, IR 4 and IR 6.

Figure 4.7 also shows the time history of the Pitot pressure, measured in the test section, simultaneously with the drag force. Note that the Pitot pressure was measured in line with the base of the cone while the forces on the cone are referenced to the tip of the model (because the forces were applied at the tip of the cone in the calibration tests). For shot 6271, the flow speed was 2470 m/s. Given the cone length of 182 mm, it will take the flow approximately 75 μs to pass from the tip of the cone to the base. To account for this, the Pitot pressure has been shifted forward in time by 75 μs relative to the drag force signal in the plots in Fig. 4.10. During the test flow the form drag on a cone would be expected to have a similar time history to the Pitot pressure (see Appendix C). It can be seen that the drag force signals follow the changes in Pitot pressure well over for the times shown, including the initial overshoot at the start and the decrease in pressure at later times.

Based on mass-spectrometry measurements in the T4 shock tunnel (Skinner, 1994) and results from a driver-gas detector (Paull, 1996), the level of contamination of the test gas by the driver gas should be less than 7.5% for the first 4 to 5 ms after flow arrival at the conditions of shot 6271. It is apparent that the tuning of the conditions for the shot sees the pressure levels start to decrease earlier than this. However, as discussed in Appendix C, the time history of drag coefficient during the test can be found from the measured drag force and Pitot pressure time histories. For the present model, the reference area for the drag coefficient, A, is taken as the base area of the cone, 7.5×10^{-3} m^2. For shot 6271, eq. (C.8)

becomes

$$C_D \approx 245 \frac{D}{p_{Pit}}, \tag{4.1}$$

where D is measured in Newtons and p_{Pit} is measured in Pa. The drag force signal obtained using IR 6 has been used with eq. (4.1) to produce the result shown in Fig. 4.12. It can be seen that, after an initial flow establishment period, the drag coefficient is approximately steady between 1 and 3 ms after flow arrival. At later times the decreasing drag coefficient is attributed to a slow increase in the pressure within the shielding that contains the stress bar. This pressure acts on the the base of the cone and decreases the nett drag force on the cone. Measurements of pressure in the base region were attempted and indicated that the base pressure increased to approximately 3 kPa 7 ms after flow arrival for shot 6271 which would account for the decrease in C_D observed in Fig. 4.12. However, reliable compensation for drag force time history using these measurements was not possible because of the low levels of pressure and the acceleration sensitivity of the gauges used.
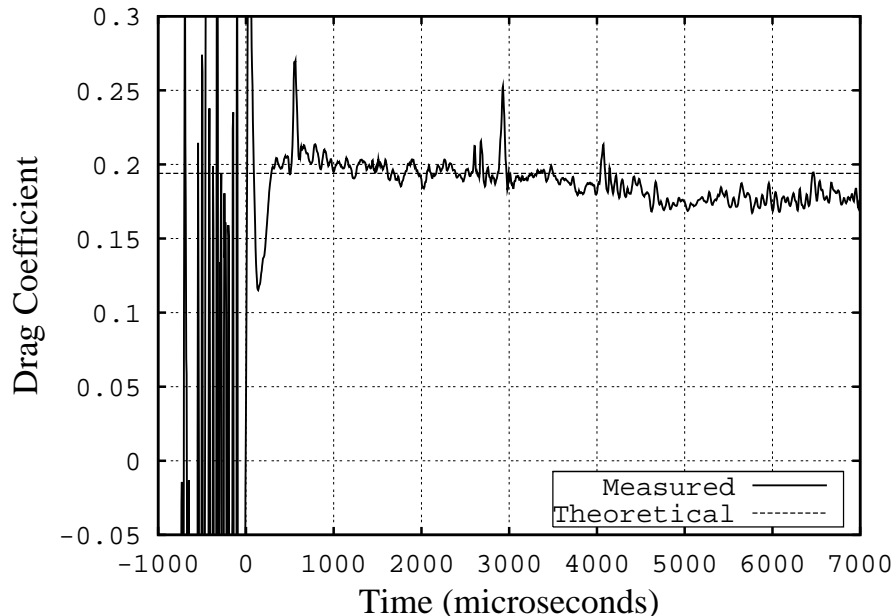

Figure 4.12: The drag coefficient, C_D, for shot 6271. D determined using IR 6.

Shown also in Fig. 4.12 is a theoretical prediction of the drag coefficient for the cone at this condition. This prediction is based on the form drag on the cone surface, determined from the surface pressure on the cone based on the theory of Taylor & Maccoll (1932). Skin friction drag is taken into account using the conditions on the cone surface from Taylor & Maccoll (1932) and assuming a laminar boundary layer. The distribution of skin-friction coefficient is based on the reference temperature method in eq. (7.45b) of White (1974). The base pressure on the cone has been assumed to be zero. The skin friction calculations are based on the flow conditions during the test time, 1 to 2 ms after flow arrival. The level predicted is close to that measured with the deviation increasing at later times as the base pressure increases.

The other three shock tunnel tests were performed at higher enthalpy conditions (refer to Table 4.2). At higher enthalpy, the flow establishment time is shorter but the duration of the test flow is terminated earlier by contamination by the driver gas than for shot 6271. Contamination times are estimated to be around 1.5 to 2.0 ms after flow start for shots 6272, 6273 and 6274 (Paull, 1996). Drag forces obtained for these shots using impulse response

IR 6 are shown in Fig. 4.13. The results are shown for only the first 2.5 ms after flow arrival because of the shorter test times. Shown again are the time histories of Pitot pressure. After a flow establishment time and prior to contamination, the drag force can be seen to follow the time history of Pitot pressure. The drag signal for shot 6272, the lower pressure condition, shows higher noise than for the higher pressure conditions. The initial dip in the drag signals for shots 6272 and 6273, just before the Pitot pressure signal rises, is associated with a spike on the piezo-film gauges that occurs at higher enthalpy conditions. Similar spikes have been observed on heat transfer instrumentation in high-enthalpy facilities (Trucco & Tamagno, 1990). The spikes occur on the strain sensor signal as the flow arrives in the test section and is attributed to ionization in the flow. These spikes are of limited duration and, since the stress waves associated with the application of aerodynamic forces on the model take some time to travel through the model and stress bar to arrive at the strain measurement location, their effect can be separated from the signal due to the aerodynamic forces by locating the strain sensor further down the stress bar (Macrossan *et al.*, 2001).
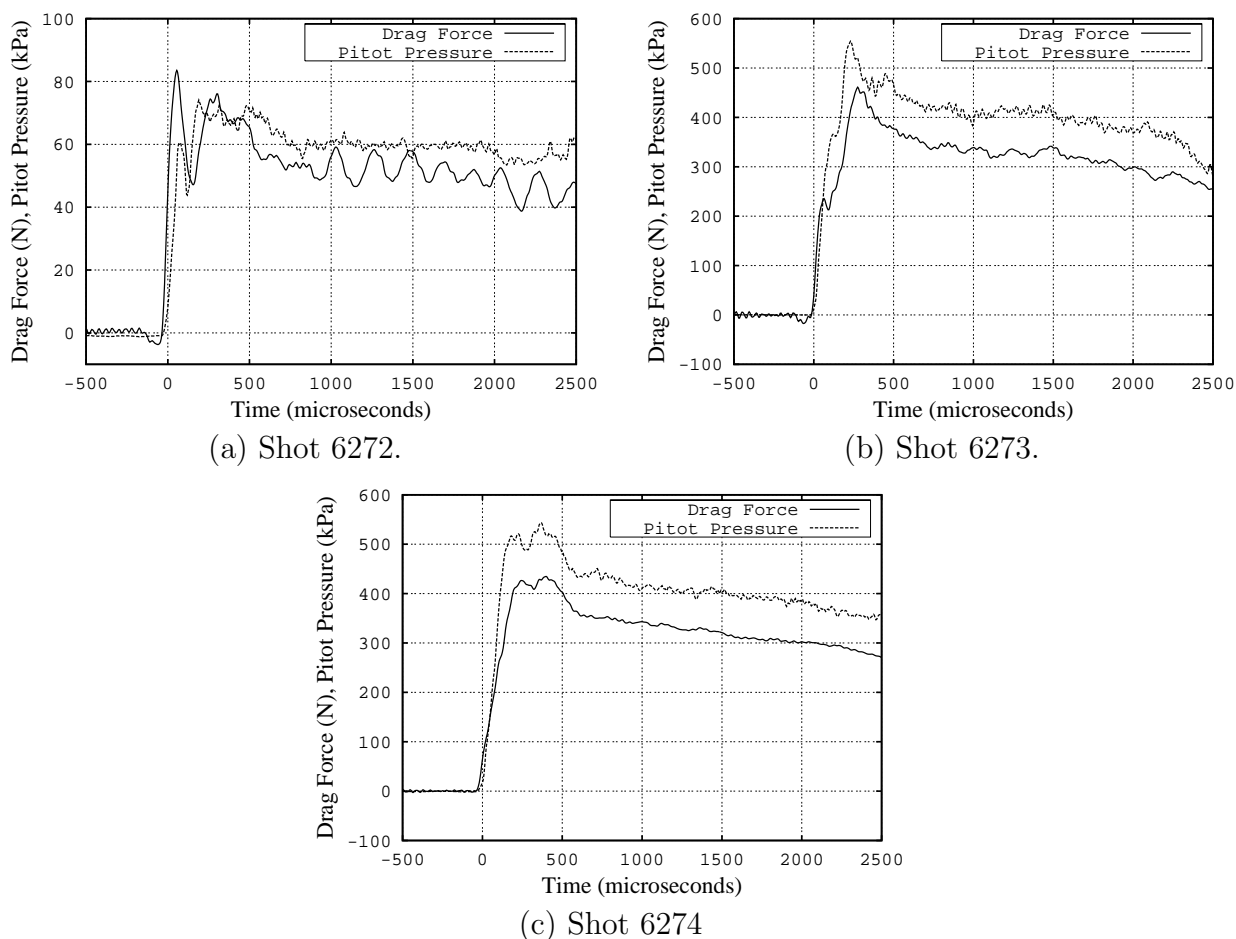

(a) Shot 6272.

(b) Shot 6273.

(c) Shot 6274

Figure 4.13: The deconvolved drag force signals (using IR 6) and Pitot pressure signals for the higher enthalpy shots.

Chapter 5

Conclusions

Different techniques for the dynamic calibration of stress wave force balance have been considered in this report. It has been shown that one or more calibration techniques may be suitable for a particular force measurement application.

For short test times, hung-weight calibration techniques can be used for freely suspended force balances. However, if the supporting arrangement for the force balance is different between the calibration tests and experiments in a wind tunnel, the effect of the supporting arrangement must be considered. The derived impulse response may be valid for a limited period of time in such cases. Free-end calibration techniques, such as self-weight or pulse tests are appropriate for cases where longer duration impulse responses are required.

The technique of cutting a fine wire either supporting a weight or supporting the model and force-balance arrangement can be used to apply a step change in load to the model. The results of deconvolving the strain signals from self-weight tests with impulse responses derived from pulse calibrations indicates that the wire cutting technique leads to a step change in load in less than 30 μs - the limit of the resolution obtained for the filtering techniques used in this report. Fine wires and sharp cutters have been found to be important when trying to produce step responses using this technique.

For cases where a high frequency response is not required, the impulse response can be determined from a pulse calibration by dividing the strain response signal by the magnitude of the impulse applied in the test. An impulse response with a higher frequency response can be obtained from a pulse test if the strain response signal is deconvolved with the measured applied pulse time-history signal.

Care needs to be taken when using pulse calibration techniques to determine impulse responses. Small errors in either the pulse signal or the strain signal can lead to large errors in the impulse response at large times.

Cross-checking the results from impulse responses derived using different calibration techniques enables any errors in the calibration procedure or processing to be clearly identified. It is recommended that such cross checks be used, where possible, to minimize potential errors in the calibration.

Acknowledgements

References

AmesResearchStaff 1953 Equations, tables and charts for compressible flow. NACA Report 1135.

Bernstein, L. 1975 Force measurements in short-duration hypersonic facilities. AGARDograph 214.

Carbonaro, M. 1993 Aerodynamic force measurements in the VKI longshot hypersonic facility. In *New Trends in Instrumentation for Hypersonic Research* (ed. A. Boutier), pp. 317–325. Dordrecht, The Netherlands: Kluwer.

Daniel, W. J. T. & Mee, D. J. 1995 Finite element modelling of a three-component force balance for hypersonic flows. *Computers and Structures* **54** (1), 35–48.

Dieulesaint, E. & Royer, D. 1980 *Elastic waves in solids - Applications to signal processing*. Chichester: Wiley.

Doebelin, E. O. 1980 *System Modeling and Response: Theoretical and Experimental Approaches*. New York: John Wiley and Sons.

Jessen, C. & Gronig, H. 1989 A new principle for a short-duration six component balance. *Experiments in Fluids* **8** (3-4), 231–233.

Joshi, M. V. & Reddy, M. N. 1986 Aerodynamic force measurements over missile configurations in IISc shock tunnel at m-infinity = 5.5. *Experiments in Fluids* **4** (6), 338–340.

Lordi, J. A., Mates, R. E. & Moselle, J. R. 1966 Computer program for numerical solution of nonequilibrium expansion of reacting gas mixtures. *Tech. Rep.* CR-472. NASA.

Macrossan, M. N., Chiu, H.-H. & Mee, D. J. 2001 A test facility for hypervelocity rarefied flows. *AIP Conference Proceedings* **585** (1), 772–779.

McIntosh, M. K. 1968 Computer program for the numerical calculation of frozen and equilibrium conditions in shock tunnels. Departmental report. Canberra, Australia.

Mee, D. J., Daniel, W. J. T. & Simmons, J. M. 1996 Three-component force balance for flows of millisecond duration. *AIAA Journal* **34** (3), 590–595.

Mee, D. J., Weiland, M. K. H. & Paull, A. 2001 Drag on a slender cone at mach 6.6 with film ejection of hydrogen. In *Proceedings of the 23rd International Symposium on Shock Waves, Fort Worth, 23-27 July, 2001*.

Morgan, R. G. & Stalker, R. J. 1983 Fast acting hydrogen valve. *Journal of Physics E - Scientific Instruments* **16**, 205–207.

NAUMANN, K. W., ENDE, H., MATHIUE, G. & GEORGE, A. 1993 Millisecond aerodynamic force measurement with side-jet model in the ISL shock tunnel. *AIAA Journal* **31** (6), 1068–1074.

PAULL, A. 1996 A simple shock tunnel driver gas detector. *Shock Waves* **6** (5), 309–312.

PAULL, A., STALKER, R. J. & MEE, D. J. 1995 Experiments on supersonic combustion ramjet propulsion in a shock tunnel. *Journal of Fluid Mechanics* **296**, 159–183.

PROST, R. & GOUTTE, R. 1984 Discrete constrained iterative deconvolution algorithms with optimized rate of convergence. *Signal Processing* **7** (3), 209–230.

REED, R. P. 1998 Convolution and deconvolution in measurement and control: Part 7 - system transient response characterization for convolution and deconvolution. *Measurements and Control* **189**, 69–83.

SANDERSON, S. R. & SIMMONS, J. M. 1991 Drag balances for hypervelocity impulse facilities. *AIAA Journal* **29** (12), 2185–2191.

SKINNER, K. A. 1994 Mass spectrometry in shock tunnel experiments of hypersonic combustion. PhD thesis, The University of Queensland.

SMITH, A. L. & MEE, D. J. 1996a Drag measurements in a hypervelocity expansion tube. *Shock Waves* **6** (3), 161–166.

SMITH, A. L. & MEE, D. J. 1996b Dynamic strain measurement using piezoelectric polymer film. *Journal of Strain Analysis for Engineering Design* **31** (6), 463–465.

SMITH, A. L., MEE, D. J., DANIEL, W. J. T. & SHIMODA, T. 2001 Design, modelling and analysis of a six-component force balance for hypervelocity wind tunnel testing. *Computers and Structures* **79** (11), 1077–1088.

TAYLOR, G. I. & MACCOLL, J. W. 1932 The air pressure on a cone moving at high speed. *Proceedings of the Royal Society (London) Series A* **139**, 278–297.

TRUCCO, R. E. & TAMAGNO, J. 1990 Elimination of an external noise spike on thin-film temperature traces. GASL Technical Memorandum 240. GASL.

TUTTLE, S. L., MEE, D. J. & SIMMONS, J. M. 1995 Drag measurements at mach 5 using a stress wave force balance. *Experiments in Fluids* **19** (5), 336–341.

WHITE, F. M. 1974 *Viscous Fluid Flow*. New York: McGraw-Hill.

Appendix A

Examples of calibration problems

In this appendix results are presented from sample calibration tests that demonstrate some of the problems simulated in section 3.2.3. These results show the sensitivity of the different calibration techniques to errors in the calibration or data-acquisition processes. They also show the importance of using multiple calibration techniques and how cross-checking can be used to identify problematical calibration tests.

A.1   Problem with cutting the wire

In calibration tests in which a fine wire is cut to provide a step removal of load, the wire cutting process can lead to errors in the impulse response. There is evidence that the cutting process in some tests leads to a force time history that deviates from that of a true step change in load on the model. This can be demonstrated by deconvolving the strain signal obtained from such a test with an impulse response determined from a valid calibration test.

The strain signal for self-weight calibration test SW205 is shown in Fig. A.1. This signal can be directly compared with the result for self-weight test SW202 in Fig. 4.2. Three differences are noted. Firstly, the initial decrease in output signal is more rapid for SW205 than for SW202 and the first minimum is more rounded than for SW202. Secondly, the magnitudes of the subsequent maxima and minima are larger for SW205 than for SW202. Thirdly, there is a small decrease in the signal level prior to the rapid drop in output voltage evident in the result for SW205. Similar drops in level are obtained in some other calibration tests involving cutting wires. Investigation of such signals indicates that such drops in signal level are not associated with the other effects discussed in this section and the influence of these drops on the inferred impulse response is not large, however, calibration tests with such results are usually discarded.

The result obtained when the strain signal from SW205 is deconvolved with impulse response IR 6, determined in section 4.2.3, is shown in Fig. A.2. The result shows that there is an initial overshoot in the indicated load that has a duration of less than one millisecond. The details of the mechanisms that lead to such overshoots as the wire is cut are not clear but such results are thought to be associated with small loads applied by the experimenter as the wire cutters are used. It has been observed that such effects can be minimized by using thinner wires and taking care not to twist the cutters as they are applied. Wire thickness is selected such that it is just larger than the minimum that can be used to support the weight. A case can be made for different methods for severing the wire, such as dedicated cutting devices, fuse-type wires, laser-based cutting, etc. However, the added complexity that such methods require has not been justified to date and results such as that for test SW205 are
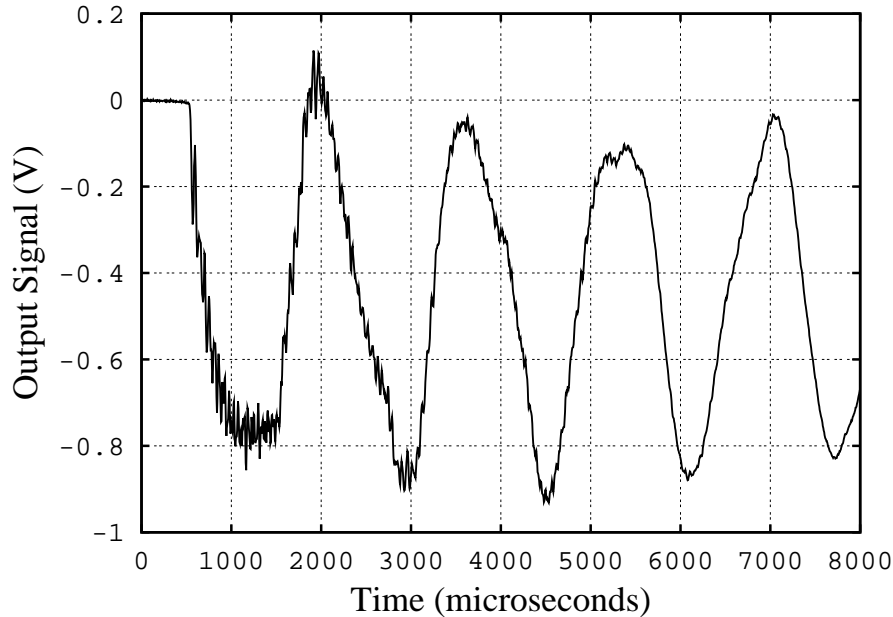
Figure A.1: Raw strain signal from self-weight test SW205.

identified and discarded as invalid calibration tests.

A.2   Non-zero regions in the pulse in a pulse test

In section 3.2.3, it was shown that small errors in the hammer pulse signal at times when the impactor is not in contact with the model (i.e. other than during the impact) can lead to errors in the impulse response derived from such a calibration test. This is demonstrated for a hammer calibration test in this section.

The hammer signal for pulse calibration test 6274H5 is shown in Fig. A.3. When looking at the hammer signal over the period that will be used to find the impulse response, Fig. A.3(a), the signal looks to be very good with low noise levels outside of the region of the pulse. However, when the vertical scale is expanded around zero, see Fig. A.3(b), it can be seen that the mean level of the signal is about -1 N outside of the region of the pulse.

The data acquisition system used to capture the signals in the present experiments (MONC) determines the zero level for each signal by taking the mean of the first 100 points of each data record. The signals for the test 6274H5 were recorded using a pre-triggering mode and there were 2192 pre-trigger samples (note that the time scales in Fig. A.3(a) and (b) start 11 ms after the start of the sampling window). The full time record of the signal captured by the data-acquisition system for test 6274H5 is shown with the vertical scale expanded in Fig. A.3(c). The noise level is about ± 1.5 N and, for a signal level of 480 N, this gives a signal-to-noise ratio in excess of 300. In this example, it happens that the first 100 samples are taken when the noise is in the positive direction, so that mean of the signal over the rest of the 40 ms record is approximately -1 N. One would expect that this would be insignificant but consider the impulse that is applied by the hammer, that occurs over about 230 μs, compared with that obtained if 1 N was applied for 8 ms. If the hammer signal is approximated as a triangular pulse of peak 480 N and base width 230 μs, then the impulse applied by the pulse would be 55 mNs. The impulse applied by 1 N for 8 ms would be 8 mNs, or approximately 14% of the impulse applied by the hammer. Thus, this small error in the hammer signal is not negligible.
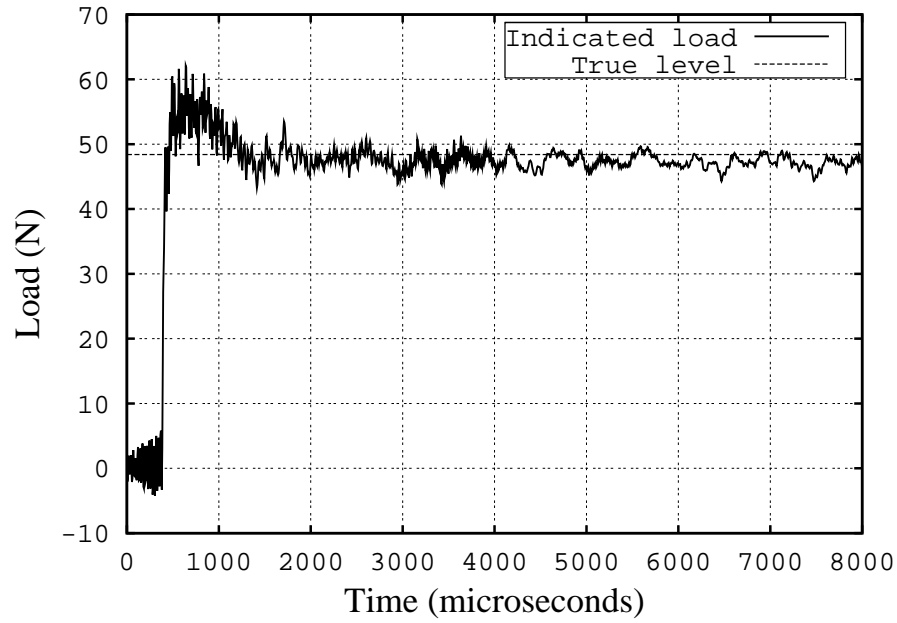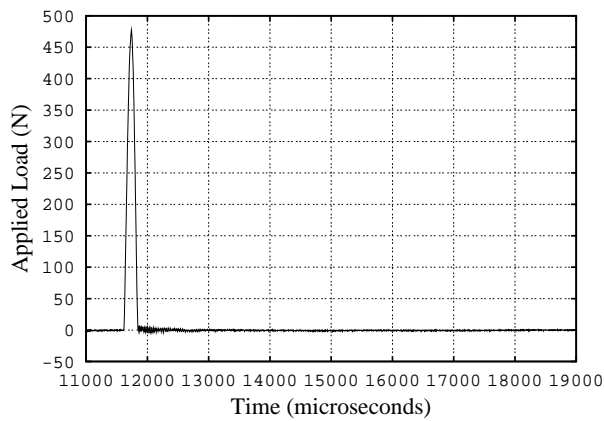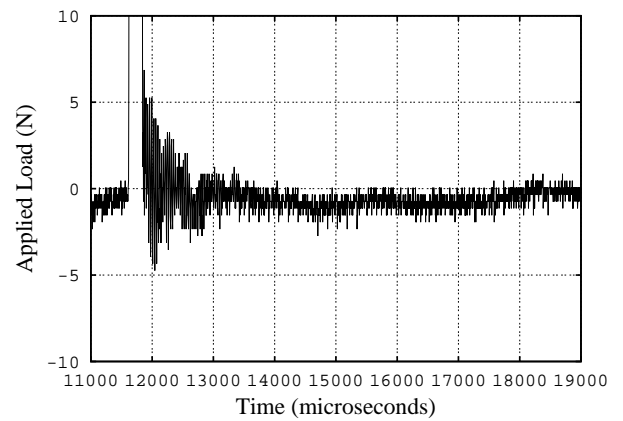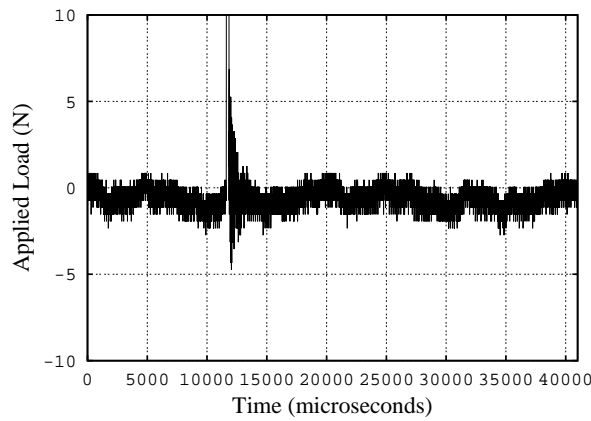
50

Figure A.2: Strain signal from test SW205 deconvolved with IR 6, 30-μs moving-average filter applied.

(a) Hammer signal

(b) Signal with vertical scale expanded.

(c) Signal over full time length, expanded vertical scale

Figure A.3: The strain signals measured for pulse calibration tests H104 and H105.

The hammer check signal, obtained as suggested in section 3.2.3 by convolving the hammer signal with a unit step, is shown in Fig. A.4. This shows that at later times the check signal deviates from being horizontal and suggests that correction of the signal may be appropriate.
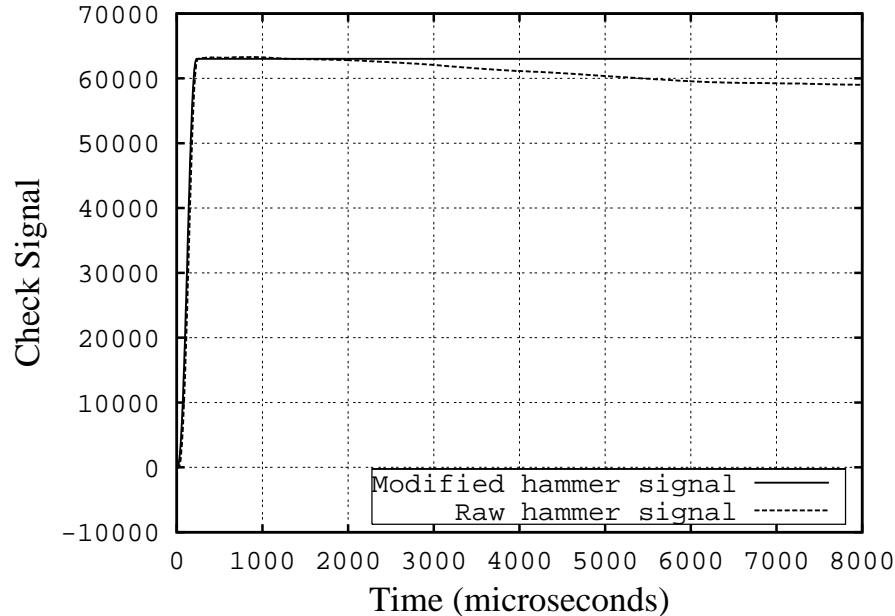

Figure A.4: Check signals for pulse calibration test 6274H5.

If an impulse response is determined using the raw hammer signal, it can be used to deconvolve the strain signal from self-weight test SW203. The result of this is shown in Fig. A.5(a). It can be seen that the recovered load deviates from the true level beyond about 3 ms after the step change in load. The hammer signal for test 6274H5 has been corrected using the procedure outlined in section 3.2.3 by setting the force to zero outside the regions of the pulse. An impulse response has also been made using this "modified" hammer signal and the strain signal from test SW203 has been deconvolved using this impulse response. The result is shown in Fig. A.5(b). There is a clear improvement in the signal beyond 3 ms after the step change in load, although there is still an error of approximately 5% at the end of the record.

A.3 Low frequency noise on strain signals in a pulse test

In section 3.2.3 it was noted that a small-amplitude, low-frequency noise on the strain signal in a pulse calibration could lead to large errors in deconvolved signals at large times. In one of the preliminary calibration tests on the force balance described in chapter 4, the strain signals on one of the strain sensors was corrupted by such noise. The results from two of the calibration tests can be used to demonstrate this effect experimentally.

Calibration tests H104 and H105 were pulse calibration tests. The pulse input for test H104 had a peak magnitude of approximately 570 N and the pulse duration was approximately 190 μs. For test H105 the peak was approximately 180 N and a slightly broader pulse of 260 μs was obtained. The strain signals measured for the two tests are shown in

(a) IR from raw hammer signal
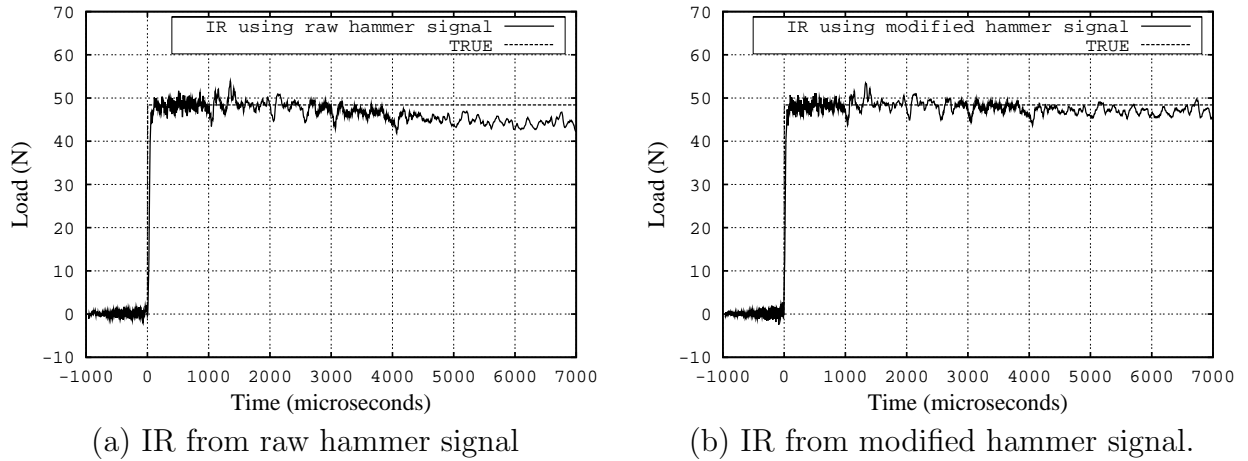
(b) IR from modified hammer signal.

Figure A.5: Strain signal from self-weight test SW203 deconvolved using impulse responses determined from pulse calibration test 6274h5.

Fig. A.6(a). The higher signal level for test H104 is associated with the larger impulse applied by the hammer. There is a small difference in the triggering so that the signal for test H104 leads that for H105. Because of the shorter pulse for test H104, the peaks in the strain signal are sharper. Apart from those differences, the signals are similar and no significant noise on the signals is apparent. However, when the pre-trigger part of the signals are examined more closely, the influence 50 Hz noise is apparent, see Fig. A.6(b). In this figure the signals have been filtered with a 50-μs moving-average filter to show the effects more clearly. The start of the signal for H104 has been captured when the 50-Hz noise is on the upward part of the cycle and that for H105 is on the downward part.[1]

(a) Raw signals.

(b) Zoom in on the first 2.5 ms.
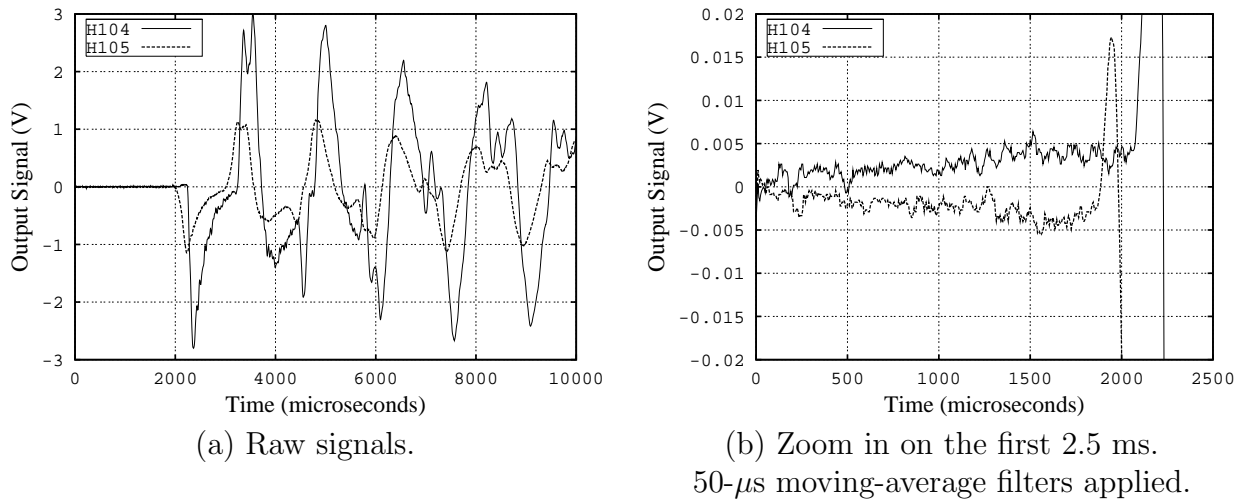50-μs moving-average filters applied.

Figure A.6: The strain signals measured for pulse calibration tests H104 and H105.

In order to examine the effects of this noise on the quality of the impulse responses

---

[1]It may also be noted that there is a short, sharp rise in strain output signals just before the negative-going signal associated with the impact. This was found to be due to electrical interference between the hammer and the strain sensor when the steel tip of the hammer makes electrical contact with the model. A study of such noise indicated that it does not affect the processed results and it could be eliminated by placing a thin layer of insulating material (tissue paper) between the hammer and the model when calibrating. Note that no such noise is present in the strain signals for the pulse calibration tests used in the experiments reported in chapter 4.

obtained from these signals, the following approach has been used.

1. The impulse responses for calibration tests H104 and H105 have been determined using the deconvolution method used to find IR6 in section 4.3.

2. Each impulse response was then convolved with a unit step to produce simulated unit step responses.

3. The step response obtained in step 2 for test H104 was deconvolved with the impulse response for test H105 in step 1.

4. The step response obtained in step 2 for test H105 was deconvolved with the impulse response for test H104 in step 1.

If the impulse responses obtained from the calibration tests are unaffected by the noise on the signals, then the deconvolutions done in steps 3 and 4 should recover the unit step load. The recovered step loads are shown in Fig. A.7. It can be seen that the recovered loads begin at the correct level (unity) but start to diverge after about 1 ms. This is the effect illustrated in the simulations in Fig. 3.24.
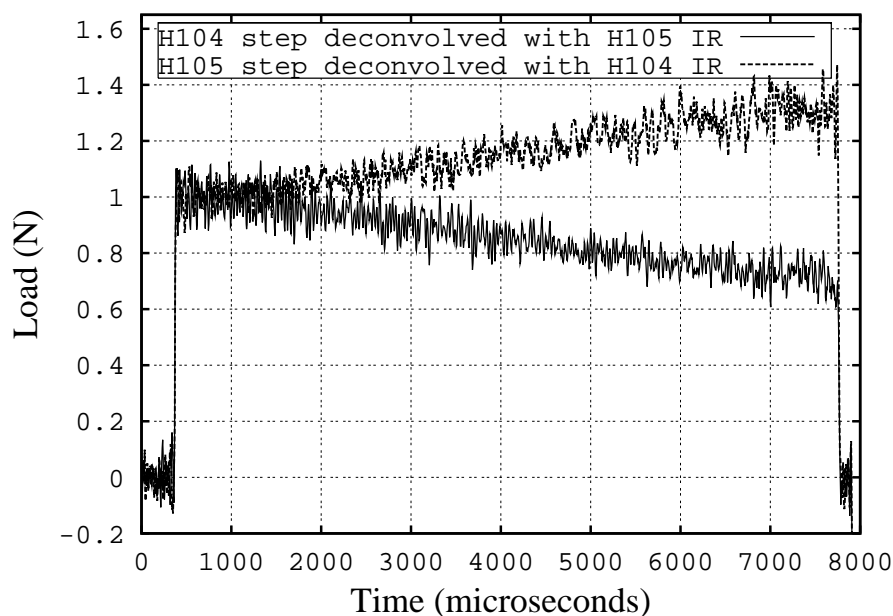

Figure A.7: Recovery of unit step inputs for cross deconvolutions for tests H104 and H105, calibration tests corrupted by low-frequency noise.

Appendix B

Calibration using impact of a pendulous mass

Consider a calibration technique in which a pendulous mass that is released from rest from its initial height, h_i, impacts the model on a stress-wave force balance, then rebounds and comes to rest at height, h_f, before striking the model a second time (see Fig. B.1). Stress waves will be initiated in the model due to the impact and, if the duration of the impact is short, the response of the balance to the impact is approximately the impulse response multiplied by the magnitude of the impulse applied during the impact, as discussed in section 2.2. Only the first impact is considered. To determine the magnitude of the impulse, only the mass of the ball, the initial height and how far back the ball bounces are required.
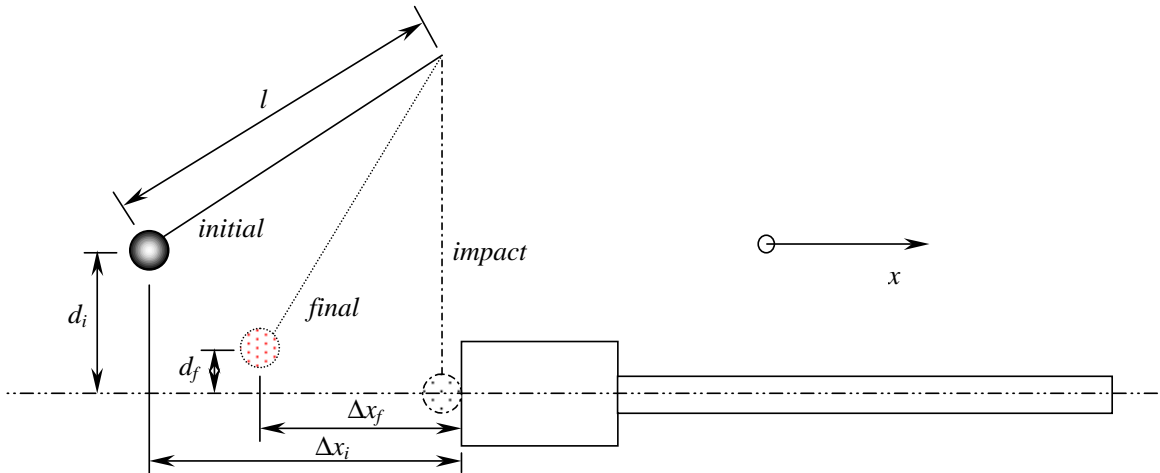

Figure B.1: Schematic diagram of pendulous mass impact calibration technique.

Consider the downward motion of the ball. The initial potential energy of the ball is mgd_i and the initial kinetic energy is zero. Immediately before impact, the speed of the ball is v, the potential energy of the ball is zero and the kinetic energy is $\frac{1}{2}mv^2$. Conservation of energy leads to the velocity of the ball immediately before impact,

$$\mathbf{v} = \sqrt{2gd_i}\mathbf{i}. \tag{B.1}$$

Consider the impact. Let the force on the ball during impact be a function of time, $\mathbf{F}(t)$. Note that this force will be in the negative x direction. Let t_1 be the time when the ball and

the model first make contact and t_2 be the time just as they separate. Let the velocity of the ball immediately after impact be $\mathbf{v}^*$. Then, conserving momentum for the ball gives

$$m\mathbf{v} + \int_{t_1}^{t_2} \mathbf{F}dt = m\mathbf{v}^*. \tag{B.2}$$

The total impulse applied to the ball during impact (that is equal but opposite to the impulse applied to the model during the impact) is then given by

$$\mathbf{I}_B = \int_{t_1}^{t_2} \mathbf{F}dt = m\left(\mathbf{v}^* - \mathbf{v}\right). \tag{B.3}$$

Consider the rebounded upward motion of the ball. Conservation of energy for the ball after impact can be used to find the velocity of the ball immediately after impact,

$$\mathbf{v}^* = -\sqrt{2gd_f}\mathbf{i}. \tag{B.4}$$

The total impulse applied to the ball is found from eqs. B.1, B.3 and B.4,

$$\mathbf{I}_B = -m\sqrt{2g}\left(\sqrt{d_i} + \sqrt{d_f}\right)\mathbf{i}. \tag{B.5}$$

The impulse applied by the ball to the model, $\mathbf{I}_M$, is in the positive x direction,

$$\mathbf{I}_M = m\sqrt{2g}\left(\sqrt{d_i} + \sqrt{d_f}\right)\mathbf{i}. \tag{B.6}$$

Geometry can be used to relate the initial and final heights to the pendulum length and the initial and final distances in the x direction of the ball from the model (refer to Fig. B.1),

$$\mathbf{I}_M = m\sqrt{2g}\left(\sqrt{l - \sqrt{l^2 - \Delta x_i^2}} + \sqrt{l - \sqrt{l^2 - \Delta x_f^2}}\right)\mathbf{i}. \tag{B.7}$$

Appendix C

Drag coefficient in terms of Pitot pressure

In short-duration impulse facilities there may be small variations in freestream flow conditions during the nominal test period. For example, waves between the piston and the end of the compression tube in a free-piston shock tunnel may lead to small fluctuations in the nozzle supply pressure which in turn lead to fluctuations in the freestream pressure and density. It is possible to account for the effects of such freestream variations on the aerodynamic forces on a model if the Pitot pressure is measured simultaneously with the aerodynamic force. This is possible for high Mach number flows because the dynamic pressure of the flow is approximately a constant fraction of the Pitot pressure. Assuming that Reynolds-number effects on the force coefficient are small for small fluctuations or variations in conditions during the test period, it is shown below that the force coefficient can be found by normalizing the aerodynamic force time history by the Pitot pressure time history with an appropriate scaling factor.

Consider an aerodynamic body that experiences a drag force, D, that may vary with time. The drag coefficient, C_D, is defined in terms of D, the freestream flow speed, v_∞, the freestream density, ρ_∞, and the reference area, A, as

$$C_D = \frac{D}{\frac{1}{2}\rho_\infty v_\infty{}^2 A}. \tag{C.1}$$

The Rayleigh-Pitot formula (AmesResearchStaff, 1953) gives the relationship between the Pitot pressure, p_{Pit}, the freestream static pressure, p_∞, the freestream Mach number, M_∞, and the ratio of specific heats of the test gas, γ, as

$$p_{Pit} = p_\infty \left[\frac{(\gamma+1)M_\infty{}^2}{2}\right]^{\frac{\gamma}{\gamma-1}} \left[\frac{\gamma+1}{2\gamma M_\infty{}^2 - (\gamma-1)}\right]^{\frac{1}{\gamma-1}}. \tag{C.2}$$

For high values of M_∞, such that $2\gamma M_\infty{}^2 \gg (\gamma-1)$, this can be approximated as

$$p_{Pit} \approx p_\infty \left(\frac{\gamma+1}{2}\right)^{\frac{\gamma+1}{\gamma-1}} \gamma^{\frac{1}{1-\gamma}} M_\infty{}^2. \tag{C.3}$$

Noting that for a thermally perfect gas, the equation of state can be written as

$$p_\infty = \rho_\infty R T_\infty, \tag{C.4}$$

where R is the gas constant and T_∞ is the freestream static temperature, and

$$M_\infty{}^2 = \frac{v_\infty{}^2}{\gamma R T_\infty},\tag{C.5}$$

eq. (C.3) can be written as

$$p_{Pit} \approx \left(\frac{\gamma+1}{2}\right)^{\frac{\gamma+1}{\gamma-1}} \gamma^{\frac{\gamma}{1-\gamma}} \rho_\infty v_\infty{}^2.\tag{C.6}$$

For $\gamma = 1.4$, this gives $p_{Pit} \approx 0.92\rho_\infty v_\infty{}^2$.

Substituting eq. (C.6) into eq. (C.1), the drag coefficient can be written as

$$C_D \approx \left[\frac{2}{\left(\frac{\gamma+1}{2}\right)^{\frac{\gamma+1}{1-\gamma}} \gamma^{\frac{\gamma}{\gamma-1}} A}\right] \frac{D}{p_{Pit}}.\tag{C.7}$$

For a given flow all terms in the square brackets are constant and the drag coefficient is a constant multiple of the ratio of drag force to Pitot pressure,

$$C_D \approx const\frac{D}{p_{Pit}}.\tag{C.8}$$

Thus, by measuring the Pitot pressure simultaneously with the force, small variations in flow conditions during an experiment can be accounted for by plotting the force coefficient. Then the force coefficient as a function of time can be written as a constant times the ratio of force to Pitot pressure.